Université de Montréal

Ionic properties, regional heterogeneity, and electrical remodeling in a mathematical model of the canine atrial action potential

par

Rafael J. Ramirez

Programme de génie biomédical

Faculté des études supérieures

Mémoire présenté à la Faculté des études supérieures

en vue de l'obtention du grade de

Maître ès sciences appliquées (M.Sc.A.)

en génie biomédical

avril, 1999

Page d'identification du jury

Université de Montréal

Faculté des études supérieures

Ce mémoire intitulé:

Ionic properties, regional heterogeneity, and electrical remodeling in a mathematical model of the canine atrial action potential

présenté par:

Rafael J. Ramirez

a été évalué par un jury composé des personnes suivantes:

Normand Leblanc - Président du jury .....

Marc Courtemanche - Directeur de recherche .....

Stanley Nattel - Codirecteur de recherche .....

Alain Vinet - membre de jury .....

Mémoire accepté le: 95.05.24

Abstract

Dogs have been used extensively to study atrial arrhythmias, but there are no published mathematical models of the canine atrial action potential (AP). To obtain insights into the ionic mechanisms governing canine atrial AP properties, I incorporated formulations of K^+, Na^+, Ca^{2+} and Cl^- currents, based on measurements in canine atrial myocytes, into a mathematical model of the AP. The rate-dependent behavior of model APs correspond to experimental measurements, and point to a central role for I_{Ca} inactivation in rate adaptation. Incorporating previously-described regional ionic current variations in the model largely reproduced AP waveforms characteristic of the corresponding right atrial regions (appendage, pectinate muscle, crista terminalis and atrioventricular ring). When the ionic alterations induced by tachycardia-dependent remodeling are incorporated, the model reproduces qualitatively the AP features associated with the substrate for atrial fibrillation in dogs exposed to chronic rapid atrial activation. In conclusion, this ionic model of the canine atrial AP agrees well with experimental measurements, gives potential insights into underlying mechanisms, and could potentially be used as a basis for simulations of propagated impulses in canine atrial arrhythmia models.

Sommaire

Les arythmies auriculaires telle que la fibrillation auriculaire (FA) représentent des anomalies cardiaques pour lesquelles le traitement demeure encore incertain. Les animaux sont utilisés comme modèle pour investiger ces manifestations et ces études ont grandement contribué à l'avancement des connaissances sur la pathogenèse de l'arythmie chez l'homme. Parmi eux, le modèle canin a été fréquemment étudié pour la FA malgré les différences marquées qui existent entre les potentiels d'action (PA) auriculaires chez l'homme et le chien. Comparées aux cellules auriculaires humaines, les cellules auriculaires de chien démontrent: (i) une diminution de l'amplitude du courant transitoire potassique (I_{to}), (ii) une altération de la cinétique et une augmentation de l'amplitude du courant ultra-rapide potassique ($I_{Kur,d}$); (iii) une diminution de 50% de l'amplitude de la composante lente du courant potassique à rectification retardée (I_{Ks}) et une augmentation de 100% de l'amplitude de la composante rapide du courant potassique à rectification retardée (I_{Kr}); et (iv) un courant chlorure activé par le calcium ($I_{Cl,Ca}$) qui n'est pas documenté chez l'homme. Ces différences résultent en une durée du PA auriculaire plus courte chez le chien. L'utilisation généralisée du modèle canin d'arythmie et les différences connues entre les PA auriculaires chez l'homme et le chien justifient le développement d'un modèle mathématique du PA auriculaire du chien pour consolider

nos connaisances sur le sujet de l'électrophysiologie auriculaire du chien et pour mieux comprendre la relation qui existe entre l'électrophysiologie de l'homme et celle du chien.

J'ai developpé un modèle mathématique de PA auriculaire de chien qui incorpore les propriétés de chacun des courants ioniques impliqués dans la génèse du PA. Les courants ioniques sont modélisés à partir d'études récentes sur les cellules auriculaires isolées. Le modèle décrit les courants ioniques transmembranaires, les pompes et les échangeurs. Les courants transmembranaires incluent I_{to}, $I_{Kur,d}$, I_{Kr}, I_{Ks}, $I_{Cl,Ca}$, le courant calcique (I_{Ca}), le courant potassique à rectification entrante (I_{K1}), et le courant sodique rapide entrant (I_{Na}).

Le modèle reproduit de nombreuses observations rapportées par d'autres études. Les simulations de protocoles en voltage imposé démontrent des courants ioniques qui correspondent aux données expérimentales. À une fréquence de 1 Hz, le modèle de PA démontre une phase de dépolarisation rapide (phase 0), une repolarisation initiale (phase 1), une phase de plateau (phase 2) autour de -15 mV, une repolarisation tardive (phase 3) suivie d'un retour au potentiel diastolique à -83 mV. La durée du PA à 95% de repolarisation (DPA_{95}) est de 201 ms, ce qui se situe dans l'intervalle observé expérimentalement.

Les cellules auriculaires canines démontrent une adaptation aux changements de la fréquence, ou une diminution de la DPA_{95} en réponse à une augmentation de la fréquence de stimulation. Le modèle du PA reproduit cette réponse; la DPA_{95} est de 252 ms à une fréquence de 0.1 Hz, et elle diminue à 131 ms à une fréquence de 5 Hz. La perte de cette adaptation aux changements de la fréquence est associée avec une augmentation de

la susceptibilité à la FA. Le comportement fréquence-dépendante du modèle suggère un rôle central de l'inactivation du courant I_{Ca} et du Ca^{2+} intracellulaire dans le processus d'adaptation aux changements de fréquence de stimulation.

Le modèle du PA auriculaire chez le chien est utilisé pour investiger l'hétérogénéité ionique des différentes régions de l'oreillette droite: le muscle pectiné, la crista terminalis, la région de la boucle auriculoventriculaire, ainsi que l'appendice auriculaire. Quand les variations des courants ioniques mesurées expérimentalement sont appliquées au modèle, les PA résultants concordent bien aux tracés des PA moyens des régions auriculaires correspondantes. Dans ce modèle mathématique ainsi que dans les données expérimentales, les PA des cellules de la crista terminalis montrent une morphologie "spike-and-dome" et une durée prolongée, tandis que les cellulles de la région de la boucle auriculoventriculaire ont une morphologie triangulaire et une courte durée. Les cellules de l'appendice et du muscle pectiné possèdent des valeurs de DPA_{95} intermédiaires. Le plateau du PA des cellules de l'appendice est légèrement élevé. La bonne corrélation entre le modèle du PA et les mesures expérimentales soutiennent la notion du substrat ionique comme médiateur de l'hétérogénéité régionale.

Les périodes prolongées de la FA contribuent à la stabilisation de l'arythmie et augmentent la susceptibilité à des épisodes subséquentes. Le mécanisme qui contribue à la nature soutenue de la FA, appelé remodelage électrique, inclut le raccourcissement de la DPA_{95} et la perte de l'adaptation aux changements de la fréquence de stimulation. Les changements ioniques associés à la stimulation auriculaire rapide (400/min) ont été

appliqués au modèle canin pour étudier le remodelage électrique induit par la FA. Les études en voltage imposé sur les myocytes auriculaires de chien suite à une stimulation auriculaire rapide stipulent que le remodelage électrique dans les myocytes isolés est associé à la réduction de la densité des courants I_{Ca} et I_{to} sans altération de la cinétique des canaux ou de leur dépendance au potentiel membranaire. Quand ces altérations sont incorporées dans le modèle, celui-ci reproduit qualitativement les caractéristiques observées expérimentalement. Cependant, le degré du raccourcissement de la DPA_{95} ainsi que la perte de l'adaptation à la fréquence observée expérimentalement ne sont pas reproduits quantitativement par le modèle.

Le modèle du PA auriculaire du chien est en accord avec de nombreux résultats expérimentaux, incluant les réponses des courants ioniques aux simulations de pulses dépolarisants, et l'adaptation du PA aux changements de la fréquence de stimulation. Les simulations du modèle suggèrent un rôle central de l'inactivation du courant I_{Ca} et du Ca^{2+} intracellulaire dans le processus d'adaptation à la fréquence et confirme le rôle des variations de courants ioniques comme médiateur de l'hétérogénéité régionale dans l'oreillette droite chez le chien. Le modèle nous fournit un outil utile pour examiner les interventions pharmacologiques et pourra être utilisé pour les simulations de propagation de PA et pour l'étude de l'initiation et de l'évolution des arythmies auriculaires.

Table of Contents

List of Tables

List of Figures

List of Abbreviations

Symbol	Definition
R	Gas constant
T	Temperature
F	Faraday constant
C_m	Membrane capacitance
AP	Action potential
$\dot{V}max$	Maximal AP upstroke velocity
APA	AP amplitude
APO	AP overshoot
APD	AP duration
APD_{90}	APD to 90% repolarization
APD_{95}	APD to 95% repolarization
AF	Atrial fibrillation
SR	Sarcoplasmic reticulum
JSR	Junctional SR (release compartment)
NSR	Network SR (uptake compartment)
V_{cell}	Cell volume
V_i	Intracellular volume
V_{up}	NSR volume
V_{rel}	JSR volume
$[X]_o$	extracellular concentration of ion X
$[X]_i$	intracellular concentration of ion X
Cmdn	Calmodulin: sarcoplasmic Ca^{2+} buffer
Trpn	Troponin: sarcoplasmic Ca^{2+} buffer
Csqn	Calsequestrin: JSR Ca^{2+} buffer
$[Ca^{2+}]_{rel}$	Ca^{2+} concentration in JSR
$[Ca^{2+}]_{up}$	Ca^{2+} concentration in NSR
$[Ca^{2+}]_{Cmdn}$	Ca^{2+}-bound calmodulin concentration
$[Ca^{2+}]_{Trpn}$	Ca^{2+}-bound troponin concentration
$[Ca^{2+}]_{Csqn}$	Ca^{2+}-bound calsequestrin concentration

Symbol	Definition
E_X	Equilibrium potential for ion X
I_{ion}	Total sarcolemmal ionic current
I_{stim}	Stimulus current
α_x	Forward rate constant for gating variable x
β_x	Reverse rate constant for gating variable x
τ_x	Time constant for gating variable x
x_∞	Steady state relation for gating variable x
I_{Na}	Fast inward Na^+ current
g_{Na}	Maximal I_{Na} conductance
m	I_{Na} activation variable
h	I_{Na} fast inactivation variable
j	I_{Na} slow inactivation variable
I_{K1}	Inward rectifier K^+ current
g_{K1}	Maximal I_{K1} conductance
I_{to}	Transient outward K^+ current
g_{to}	Maximal I_{to} conductance
o_a	I_{to} activation variable
o_i	I_{to} inactivation variable
$I_{Kur,d}$	Ultrarapid delayed rectifier K^+ current
$g_{Kur,d}$	Maximal $I_{Kur,d}$ conductance
u_a	$I_{Kur,d}$ activation variable
u_i	$I_{Kur,d}$ inactivation variable
I_{Kr}	Rapid delayed rectifier K^+ current
g_{Kr}	Maximal I_{Kr} conductance
x_r	I_{Kr} activation variable
I_{Ks}	Slow delayed rectifier K^+ current
g_{Ks}	Maximal I_{Ks} conductance
x_s	I_{Ks} activation variable
I_{Ca}	Inward Ca^+ current
g_{Ca}	Maximal I_{Ca} conductance
d	I_{Ca} activation variable
f	I_{Ca} voltage-dependent inactivation variable
f_{Ca}	I_{Ca} Ca^{2+}-dependent inactivation variable
I_{NaCa}	Na^+/Ca^{2+} exchanger current
$I_{NaCa(max)}$	I_{NaCa} scaling factor
$I_{p,Ca}$	Sarcoplasmic Ca^+ pump current

Symbol	Definition
I_{NaK}	Na^+-K^+ pump current
$I_{NaK(max)}$	Maximal I_{NaK}
f_{NaK}	Voltage-dependence parameter for I_{NaK}
σ	$[Na^+]_o$-dependence parameter for I_{NaK}
$K_{m,Na(i)}$	$[Na^+]_i$ half-saturation constant for I_{NaK}
$K_{m,K(o)}$	$[K^+]_o$ half-saturation constant for I_{NaK}
$I_{Cl,Ca}$	Ca^+-activated Cl^- current
q_{Ca}	Ca^{2+} flux-dependent activation gating variable for $I_{Cl,Ca}$
$K_{m,Na}$	$[Na^+]_o$ saturation constant for I_{NaCa}
$K_{m,Ca}$	$[Ca^{2+}]_o$ saturation constant for I_{NaCa}
k_{sat}	Saturation constant for I_{NaCa}
γ	Voltage-dependence parameter for I_{NaCa}
$I_{b,Na}$	Background Na^+ current
$g_{b,Na}$	Maximal $I_{b,Na}$ conductance
$I_{b,Ca}$	Background Ca^+ current
$g_{b,Ca}$	Maximal $I_{b,Ca}$ conductance
I_{rel}	Ca^+ release current from the JSR
k_{rel}	Maximal Ca^{2+} release rate for I_{rel}
u	Activation gating variable for I_{rel}
v	Ca^{2+} flux-dependent inactivation gating variable for I_{rel}
w	Voltage-dependent inactivation gating variable for I_{rel}
F_n	Sarcoplasmic Ca^{2+} flux signal for I_{rel}
I_{up}	Ca^{2+} uptake current into the NSR
$I_{up(max)}$	Maximal Ca^{2+} uptake rate for I_{up}
$[Ca^{2+}]_{up(max)}$	Maximal Ca^{2+} concentration in NSR
I_{tr}	Ca^{2+} transfer current from NSR to JSR
τ_{tr}	Ca^{2+} transfer time constant
$I_{up,leak}$	Ca^{2+} leak current from the NSR
$[Cmdn]_{max}$	Total calmodulin concentration in myoplasm
$[Trpn]_{max}$	Total troponin concentration in myoplasm
$[Csqn]_{max}$	Total calsequestrin concentration in JSR
$K_{m,Cmdn}$	Ca^{2+} half-saturation constant for calmodulin
$K_{m,Trpn}$	Ca^{2+} half-saturation constant for troponin
$K_{m,Csqn}$	Ca^{2+} half-saturation constant for calsequestrin
V_{rest}	Resting membrane potential
z	Valence

Chapter 1

Introduction

1.1 Atrial Fibrillation

Atrial fibrillation (AF) is the most frequently encountered cardiac arrhythmia in clinical practice. It is characterized by disorganized, irregular and unsynchronized electrical activity, and results in loss of atrial contractility. Atrial fibrillation, whose incidence increases strongly with age, is not a fatal arrhythmia; however, the presence of AF has a wide range of negative effects. AF may trigger ventricular tachyarrhythmias, affect cardiac function, and presents a risk for thromboembolic complications [48].

The mechanism most likely responsible for AF is the presence of multiple activation wavelets in the atria, as originally proposed by Moe [45]. The multiple wavelet hypothesis accounts for key features of AF: vulnerability of atrial tissue to AF is related to heterogeneity of atrial refractoriness, premature excitation may serve as a trigger for fibrillatory episodes, and there is a vulnerable period during the early refractory period of the tissue.

Abbreviated refractoriness favors the initiation and maintenance of AF [1, 48]. Thus, pharmacologic treatment of AF seeks to prevent or terminate AF by prolonging refractoriness. Prolonged refractoriness increases reentry wavelength, which is the minimal

circuit size permitting reentry (measured as the product of the refractory period and conduction velocity). An increased reentry wavelength reduces the number of functional reentrant circuits necessary to sustain AF, thus terminating it.

1.2 Experimental Animal Models

The limited feasibility of human tissue studies, due to restricted availability or ethical matters, stresses the importance of practical animal models in which to study normal and arrhythmic properties of cardiac function. Experimental models have provided a clearer understanding of atrial electrophysiology and have improved treatment and prevention of arrhythmias such as AF. Activation mapping studies of the canine atria provided the first evidence for Moe's multiple wavelet hypothesis [2]. Important contributors to AF vulnerability are heterogeneity of refractoriness [5, 38, 50] and loss of adaptation to changes in rate [3]. Regional heterogeneity increases the degree of fractionation of activating wavefronts, while the decreased refractoriness increases the number of possible wavefronts.

Studies in chronically instrumented goats have shown that AF induces changes in the electrophysiologic properties of the atria, which contribute to the progressive vulnerability of the atria to AF, thus the phrase, "AF begets AF" [69]. This self-perpetuating nature of AF via changes in the electrophysiologic properties has been termed electrical

remodeling. The changes caused by electrical remodeling include a shortening of the effective refractory period, a loss of adaptation to changes in rate, reduced AF cycle length, and an increase in the inducibility and stability of AF [69]. At the cellular level, electrical remodeling in a canine tachycardia model of AF is manifest via reductions in both the sarcolemmal calcium current, I_{Ca}, and the transient outward potassium current, I_{to} [73]. Mapping studies in closed chest dogs [25] and goats [59], and clinical trials in patients with chronic AF [60] are consistent with the notion that intracellular calcium overload mediates electrical remodeling.

Voltage-clamp studies of atrial myocytes give us an indication of how different ion channels respond under different conditions and how the contribution of these currents may change at the level of the action potential. Activation mapping studies give us an idea of how action potential alterations might affect propagation and contribute to the initiation and maintenance of arrhythmias. There has been speculation about how ionic current changes may contribute to the substrate for AF [73]. There is a need for further work to clarify the electrophysiological abnormalities associated with AF and especially to determine the relationships among changes observed at different levels of study: the ion channel, the action potential (AP), and impulse propagation *in vivo*.

1.3 Statement of Problem

Atrial fibrillation is the most frequently encountered cardiac arrhythmia, whose prevention and treatment remains difficult. The potential risk factors associated with AF underline the importance of developing effective treatments. This importance is further emphasized by the association of incidence with age, and the current trend of an aging population. Similarities between dog and human atrial electrophysiology make canine atria the most practical tissue source for *in vivo* experimental studies of atrial fibrillation. There is an expanding body of knowledge of dog-specific data pertaining to mechanisms and treatment of AF, and about ionic currents in dog atrial cells in normal and diseased conditions. However, there is a great need for quantitative approaches to relate ionic current data, from single-channel and single-cell studies, to AP properties and electrical propagation.

The consolidation of results from different areas of research is often problematic. Mathematical modeling provides a quantitative approach that addresses this problem. Mathematical models allow for the testing of ideas about the importance of individual ion channels, ionic currents, and disease- and arrhythmia-induced alterations, in controlling AP properties and arrhythmic processes. Furthermore, mathematical models can complement experimental research by revealing potential avenues for new investigation.

1.4 Objectives

The goal of this work is, therefore: (i) to develop a mathematical model of the canine atrial action potential, and (ii) to use this model to investigate certain observations that are not easily amenable to experimental analysis because of technical limitations. Observations for which the ionic basis is to be analyzed include regional AP heterogeneity and AP changes in AF-induced electrical remodeling.

The remainder of this chapter outlines previous work that forms the basis for this study. Section 1.5 gives an overview of experimental results obtained in single cell studies of ionic currents. A more detailed review of the specific experimental sources of data that were used to formulate the mathematical canine atrial AP model is provided in chapter 2. Section 1.6 surveys prior mathematical models of action potentials. Section 1.7 presents experimental studies related to atrial fibrillation, in particular, regional heterogeneity and AF-induced electrical remodeling, which will be examined using the canine atrial AP model.

1.5 The Atrial Myocyte

Several recent studies have characterized the properties of ion channels specific to canine atrial tissue. The atrial action potential represents the result of integrated ionic currents across the cell membrane, carried principally by Na^+, K^+, Ca^{2+}, and Cl^- ions. Several of

these currents are well characterized in canine atria, including the transient outward K^+ current (I_{to}) [71], the dog-specific, ultrarapid delayed rectifier K^+ current ($I_{Kur,d}$) [72], the rapid and slow components of the classical K^+ delayed rectifier (I_{Kr} and I_{Ks}) [71], the sarcolemmal Ca^{2+} current (I_{Ca}) [17, 73], and the Ca^{2+}-activated Cl^- current ($I_{Cl,Ca}$) [71].

The time-dependent transient outward K^+ current, I_{to}, was first characterized in detail in canine atrial myocytes by Yue *et al* [71] using the whole-cell voltage-clamp method. I_{to} is a rapidly activating and inactivating repolarizing current that plays a prominent role in initial (phase 1) repolarization of the action potential [17, 34, 71, 72, 73].

The dog-specific, ultrarapid delayed rectifier K^+ current, $I_{Kur,d}$, exhibits activation kinetics similar to I_{to} [72], and also plays a role in the initial repolarization of the AP. $I_{Kur,d}$ can be separated from I_{to} by virtue of its sensitivity to micromolar concentrations of 4-aminopyridine. Unlike I_{to}, inactivation of $I_{Kur,d}$ is very slow (about two orders of magnitude slower than I_{to} around plateau potentials) [17, 34, 72, 73]. This slow inactivation allows $I_{Kur,d}$ to contribute to the control of the duration of the AP plateau, in a balance with the sarcolemmal calcium current, I_{Ca}.

The rapid and slow components of the delayed rectifier K^+ current, I_{Kr} and I_{Ks}, activate orders of magnitude slower than I_{to} or $I_{Kur,d}$, and thus mediate the late repolarization (phase 3) of the AP. The rapid component, I_{Kr}, displays inward rectification at potentials above +10 mV and has a small current density (typically below 1.5 pA/pF), which often makes it difficult to resolve experimentally [34, 71]. The two components are

differentiated by the selective block of I_{Kr} using drugs like dofetilide and E-4031.

The sarcolemmal Ca^{2+} current, I_{Ca}, plays an important role in AP properties. Calcium-induced calcium release requires I_{Ca} influx to trigger an amplified increase in intracellular calcium concentration via release from the sarcoplasmic reticulum (SR), which is central to cellular contractility. Additionally, calcium can play an important role in several second messenger pathways. The plateau phase of the canine atrial AP represents mainly a balance between I_{Ca} and $I_{Kur,d}$. Activation and inactivation of I_{Ca} show time- and voltage-dependence [17, 34, 73]. Although inactivation of I_{Ca} is mediated predominantly by intracellular calcium concentration [58].

The time-independent inward rectifier K^+ current, I_{K1}, is often measured as a barium-sensitive inward current. I_{K1} maintains the negative resting membrane potential in the quiescent cell [73], and assists in late (phase 3) repolarization of the AP [20].

Canine atrial myocytes exhibit a Ca^{2+}-activated Cl^- current, $I_{Cl,Ca}$, that is not observed in human atrial myocytes [35]. This current is ligand-gated [10, 74], appears and disappears very rapidly during a voltage step [71, 73], and plays a role in initial repolarization of the AP[75]. This current is dependent on intracellular calcium, but disappearance of this current is much faster than the decay of the $[Ca^{2+}]_i$-transient. Specific gating properties for $I_{Cl,Ca}$ are not well understood in canine atrial myocytes; however, the appearance of $I_{Cl,Ca}$ is associated with SR calcium release in canine ventricle [75]. A possible explanation for channel gating in $I_{Cl,Ca}$ involves a localized calcium flux in a region closely associated with the coupled sarcolemmal I_{Ca} channels and the calcium

release (I_{rel}) channels. This would account for the rapid channel kinetics and the association of $I_{Cl,Ca}$ with I_{rel}. The current-voltage relation for $I_{Cl,Ca}$ is bell-shaped, with current density decreasing at potentials positive to +40 mV [71, 73] approaching the reversal potential for I_{Ca}.

Pharmacological and electrophysiological techniques enable single-channel and single-cell studies to characterize individual ionic currents by suppressing contaminating currents. In this way, the relationship of each current to the AP can be identified. However, attempts to then consolidate those characterizations into a quantitative reconstruction of the AP in order to verify their relationships poses a challenge for experimentalists. Mathematical models of the action potential have been useful as one such approach.

1.6 Mathematical AP Models

1.6.1 General AP Models

Hodgkin and Huxley employed an empirical approach to describe quantitatively the electrical responses of the giant squid axon. Their formulations of ionic currents were sufficient to make valid predictions about major features of squid axon excitability such as AP morphology and conduction velocity [29]. The Hodgkin-Huxley model established a quantitative approach to studying ion channels by introducing channel activation and

inactivation, or channel gating, and in doing so, provided a lasting impetus for mathematical modeling of action potentials.

We now have a more complete understanding of ion channels and the electrical events that govern the action potential in a variety of specialized cells in several different species. Since the Hodgkin-Huxley model, a number of increasingly comprehensive models have been described. Many cardiac cell types have received attention in the form of mathematical models. Models of the rabbit sinoatrial (SA) node have been published by several groups [8, 13, 51, 70] who used formulations of Na^+, K^+, and Ca^{2+} currents to simulate intrinsic pacemaking activity. Electrical activity of Purkinje fibres was described in models by McAllister, Noble and Tsien [43], and DiFrancesco and Noble [14]. Beeler and Reuter [4] formulated a mammalian ventricular AP model composed of four sarcolemmal ionic currents. Luo and Rudy introduced a mammalian ventricular AP model based on data obtained from guinea pig ventricular myocytes [40, 41].

A number of models specific to atrial myocytes have been published. Rasmusson *et al* formulated a model of the bullfrog atrial cell [55]. This model did not take into account intracellular calcium handling by the SR, and lacked currents to mediate initial (phase 1) repolarization. The rabbit atrial AP model of Lindblad *et al* [39] reproduced well the properties of rabbit atrial myocytes, but species differences limit its applicability to the dog and more so, the human. Two models of the human atrial AP have been recently published: the Nygren, Fiset, Firek, *et al* (NFF) model [52]; and the Courtemanche, Ramirez, Nattel (CRN) model [11].

1.6.2 Human Atrial AP Models

The NFF and CRN human atrial AP models use a similar set of ionic currents to describe the activity of the space-clamped human atrial myocyte, yet there are several differences in the implementation of currents that separate the two models. In the NFF model, I_{Na} has a slower inactivating component, making initial repolarization slightly longer in the NFF than in the CRN model. The rapid outward K^+ currents, I_{to} and I_{Kur} in the CRN model, and I_t and I_{sus} in the NFF model, show similar combined responses to depolarizing test pulses. However, inactivation kinetics for I_{sus} in the NFF model range from 300 to 350 ms between -100 and 100 mV; while in the CRN model, the inactivation time constant for I_{Kur} increases from about 100 ms at 50 mV to several seconds at potentials negative to -40 mV. Recent characterization of I_{Kur} using prolonged (50 s) pulses in isolated human atrial myocytes has revealed a biexponential time course of I_{Kur} inactivation displaying fast and slow time constants around 1 and 7 seconds at potentials between 0 and 50 mV [18].

The human AP models implement I_{Ca} inactivation differently. A quantitative characterization of the inactivation distribution of I_{Ca} between the voltage and calcium-dependent components has not been fully defined. Ample evidence shows that I_{Ca} inactivation in human atrial myocytes has biexponential kinetics [36, 58] and exhibits voltage- and Ca^{2+}-dependence [58]. The Ca^{2+}-dependent component of inactivation is known to have a faster time course and plays a greater role than pure-voltage dependent

I_{Ca} inactivation in human atrial myocytes [58]. Evidence in isolated human atrial myocytes suggests that I_{Ca} inactivation is governed by three kinetic phases: a fast and slow Ca^{2+}-dependent component, and a much slower pure-voltage dependent component [58].

The NFF model uses two modes of I_{Ca} inactivation, fast and slow, to mediate bi-exponential decay. Both inactivation gating variables share the same voltage-dependent steady state, but their time constants, which are bell-shaped, differ by one order of magnitude. A local Ca^{2+} concentration is measured in a small subsarcolemmal domain that approximates the close coupling between the peripheral JSR and the sarcolemmal I_{Ca} channels. This measurement determines, by way of a Michaelis-Menten relationship, the proportion of sarcolemmal I_{Ca} channels in either the fast or slow inactivation state. The slow component approximates the Ca-dependent inactivation, while the fast component represents the voltage-dependent inactivation, contrary to experimental evidence which suggests a slower voltage-dependent component to inactivation [58]. Despite good I-V agreement of model and experimental I_{Ca}, no results are available for the NFF model that show I_{Ca} responses to depolarizing voltage steps.

The CRN model explicitly separates the voltage- from the calcium-dependent inactivation of I_{Ca}. Calcium-dependent inactivation uses a Michaelis-Menten relationship between bulk intracellular calcium and calcium-dependent inactivation, which displays rapid kinetics (time constant = 2 ms) as implemented by Friedman [21]. Voltage-dependent inactivation kinetics are much slower (250 - 450 ms) than that for Ca^{2+}-dependent inactivation, in agreement with experimental observations [58].

The final major difference between the NFF and CRN human atrial AP models is the initial, or resting configuration of the model. The CRN model begins simulations from a stable resting condition, allowing twelve seconds of pacing to remove any transient changes that occur in current kinetics. The NFF model is designed to give stable oscillatory conditions at a pacing frequency of 1 Hz. As outlined in the Limitations section in chapter 3, mathematical models that maintain a materials balance of ion concentrations, such as the NFF and CRN models, will generate a charge accumulation over long periods of continuous pacing as a result of a numerical design that is prevalent in these models [27, 61]. As mentioned in the CRN model, this conservation principle effect does not significantly affect short-term simulations (less than ten minutes). But since the NFF model uses an initial steady state that is stable at 1 Hz, this conservation effect is unavoidable. The NFF model addresses this problem of charge accumulation by implementing an "electroneutral Na^+ flux" that balances out the stimulus charge. The authors rationalized this "electroneutral Na^+ flux" as a possible consequence of electroneutral coupled transport mechanisms, such as Na^+-H^+ exchange and Na^+-K^+-2Cl cotransport.

1.6.3 Dog Atrial APs and Previous AP Models

Ionic current properties differ among species, resulting in differences in AP morphology. Dog atrial APs exhibit a shorter APD_{95} than in human atria (about 200 ms for dog at 1 HZ, compared with about 360 ms in humans at 1 Hz), but longer than in rabbit atria (about 100 ms at 1 Hz) [64]. The initial repolarizing K^+ currents, I_{to} and $I_{Kur,d}$,

have similar activation kinetics in dog and human atrial myocytes [65, 72]. The voltage-dependent (slow) inactivation of I_{Ca} is faster in canine atrial myocytes than in human [34, 58, 73]. Despite similarities in delayed rectifier currents, the differences in I_{Ca}, I_{to} and $I_{Kur,d}$ affect the positioning of the plateau, and as a result, can affect I_K voltage-dependent recruitment over the course of an AP. Unlike in human atria, canine atrial APs display $I_{Cl,Ca}$. This current can further contribute to initial repolarization of the canine myocyte [35] and affect APD. Contrastingly, the rabbit atrial AP has a duration about half that in canine atrial cells [64]. Rabbit atria have negligible I_{Ks} [47], but a larger initial repolarizing I_{to} [19], making repolarization very different between rabbit and dog, especially in terms of rate-adaptation effects [19]. Dog atria represent the principal tissue which has been used to study human atrial arrhythmias. However, the ionic differences between canine and human, and canine and rabbit atrial AP properties are significant enough to preclude the use of a human or rabbit atrial AP model to study canine atrial AP properties. Despite the availability of canine-specific data and the predominant use of dog models in studies of AF, there is no published mathematical model depicting the canine atrial action potential.

1.7 Experimental Arrhythmia Models

1.7.1 Regional Heterogeneity

Garrey first suggested, in 1914, that atrial fibrillation was associated with excitation block [22]. Noting contractile responses in cardiac tissue from several different animals, Garrey reasoned that generation of multiple local reentry circuits in a sufficiently large tissue mass was responsible for what he termed "fibrillary (*sic*) contraction". In 1962, Moe's multiple wavelet theory of atrial fibrillation also stressed the importance of a critical tissue size, and emphasized the relationship between AF maintenance and atrial heterogeneity of refractoriness [45]. A possible substrate for this regional heterogeneity was shown experimentally, in 1998, to stem from distinct regional ionic differences in canine atria by Feng *et al* [17] who used whole-cell patch-clamp techniques to identify ionic differences among four distinct regions in the canine right atrium: pectinate muscle, crista terminalis, appendage, and the atrioventricular (AV) ring region. Despite a large variation in individual AP morphologies, digitally averaged APs of several recordings from each region were distinct. Myocytes from the crista terminalis displayed APs with a prominent spike and dome morphology, and durations (APD_{50} and APD_{95}) that were significantly longer than in the other regions. Conversely, cells from the AV ring region were generally triangular in morphology and had the shortest AP durations. Myocytes from the pectinate muscle and the appendage regions displayed intermediate AP durations, and morphologies exhibiting a level plateau. The digitally averaged plateau phase

in appendage cells was notably elevated (displaying a more positive potential), compared to the other regions, without displaying the prominent spike and dome morphology characteristic of crista myocytes.

The analysis of ionic currents from myocytes in each region revealed that regional differences appeared consistent with the observed changes in AP morphology. The voltage- and time-dependence of ionic currents did not vary between regions, suggesting that regional differences were due to variations in relative current amplitude. I_{Ca} density was 58% greater in crista terminalis myocytes compared to other regions. Such a difference would contribute to APD prolongation and raise the plateau potential, possibly yielding an AP with a spike and dome morphology. Cells from the AV ring region had a mean I_{Ca} density that was significantly reduced compared to all other regions as well as a significantly increased I_{Kr} density. These differences would contribute to APD shortening observed in APs in this region, consistent with the triangular morphologies observed. The only reported ionic differences between the pectinate and appendage regions was a smaller I_{to} density in appendage cells, which again appeared consistent with recorded AP morphologies from the two regions.

This study by Feng *et al* confirmed a systematic regional heterogeneity of ionic currents and suggested that these regional differences may be responsible for the corresponding regional variation in AP morphology. Quantitative proof that these ionic differences were sufficient to account for the observed heterogeneity, however, was not readily amenable to experimental tests.

1.7.2 AF-Induced Electrical Remodeling

Acute atrial fibrillation can be induced by burst pacing using closely spaced electrodes, with spontaneous recovery of sinus rhythm usually occurring within seconds. When induced AF is maintained continuously, however, the duration of induced AF episodes increases, refractory period shortens and adaptation of refractory period to changes in rate is diminished [69]. We now understand that prolonged maintenance of AF induces electrical remodeling that promotes induction and stabilization of the arrhythmia. This self-sustaining nature of AF is conveyed in the phrase, "AF begets AF" [69].

Canine models employing chronic rapid atrial pacing result in dilation and increased susceptibility to sustained AF [46]. Such models are often used to investigate atrial pathologies associated with sustained AF, including electrical remodeling. Yue *et al* examined the ionic basis of electrical remodeling in atria from dogs subjected to sustained rapid atrial pacing (400/min) [73]. Prolonged rapid pacing was associated with increased sustainability of induced AF episodes, reduced refractoriness and reduced adaptation of refractoriness to changes in rate. Whole-cell patch-clamp examination of canine atrial myocytes after 0, 1, 7, and 42 days of chronic rapid atrial pacing revealed ionic changes that occurred over the course of pacing. Relative densities of I_{Ca} and I_{to} progressively decreased as rapid pacing duration increased. After 42 days, I_{Ca} was reduced by 69% and I_{to} by 65%. There were no changes in the voltage-dependence or kinetic properties of I_{Ca} or I_{to} accompanying the reductions in current density. Exposure of control cells to

high concentrations of nifedipine (10 μM) produced APD changes similar to those caused by rapid pacing. These results suggested that reductions in I_{Ca}, as a result of chronic rapid atrial pacing, decreased APD and APD adaptation to changes in rate. However, all blocking drugs are impure probes, and quantitative proof that I_{Ca} reduction is sufficient to mediate changes in AP properties, as observed in the rapid pacing model, is not feasible using standard electrophysiologic techniques.

Properties of the canine atrial action potential have been characterized on several levels: the single channel, the single cell, activation propagation in the atria and heart, and the whole organism. As a first step in addressing the problem of quantitatively integrating these results, I have developed a mathematical model of the canine atrial AP. This model is based, whenever possible, on experimental data obtained in canine atria. The model reproduces ionic current properties similar to those observed in the laboratory and includes descriptions for I_{to}, $I_{Kur,d}$, I_{Kr}, I_{Ks}, I_{K1}, I_{Ca}, and $I_{Cl,Ca}$. The model AP shows adaptation to rate between 0.1 and 5 Hz that agrees well with experimental findings, and points to I_{Ca} as a central mediator of this adaptation. Once formulated, the model is used to investigate the ionic basis for atrial regional heterogeneity and AF-induced electrical remodeling.

Chapter 2

Canine AP Model

Mathematical analysis of ionic determinants of canine atrial action potentials: rate, regional factors and electrical remodeling.

2.1 Introduction

Atrial arrhythmias such as atrial fibrillation (AF) represent common clinical problems that remain difficult to treat. Dog models have been used widely to study atrial arrhythmia mechanisms [49]. *In vivo* experiments have provided useful insights into the role of atrial tachycardia-induced remodeling [69], electrical heterogeneity [16] and pathological alterations [6, 7] in promoting the occurrence of atrial reentrant arrhythmias. More recently, patch clamp studies in isolated canine atrial myocytes have clarified the properties of a variety of ionic currents in dog atrium [71, 72, 73], and suggested ionic mechanisms for regional variations in action potential (AP) properties [17] and tachycardia-induced AP remodeling [73]. It is of great interest and potential importance to link these two levels of observation to determine the ionic mechanisms that control the occurrence of arrhythmias *in vivo*.

Pharmacological tools can be used to evaluate the roles of individual ionic currents [71, 72, 73]. However, the lack of specificity of pharmacological probes and the potential effects of interactions between currents (via voltage-dependence) pose potential limitations when interpreting results from pharmacologic studies. Detailed understanding of the mechanisms underlying normal electrophysiology and arrhythmogenesis is greatly facilitated by a quantitative approach involving mathematical modeling. Mathematical models of the AP based on formulations of ionic currents, pumps and exchangers have provided insights into properties of rabbit atrial [39] and sinoatrial node [13], guinea pig ventricular [41], bullfrog atrial [55], and Purkinje fiber [43] APs. More recently, models of the human atrial AP have been published [11, 52]. These models can account for a number of behaviors of the human atrial AP, and have also been used to analyze the effects of tachycardia-induced remodeling and to predict the consequences of selective K^+ channel blockade [12].

There is no published mathematical model of the canine atrial AP. Such a model would be valuable to interpret better the extensive information available about atrial arrhythmias *in vivo* in the dog and to consolidate the increasing body of knowledge regarding canine atrial ionic mechanisms. Mathematical analysis permits quantitative evaluation of various hypotheses regarding the mechanisms underlying electrophysiological properties and arrhythmia generation in the normal dog heart and in several well-established canine models of atrial pathology. In the present study, we develop a mathematical model of the canine atrial AP using information regarding ionic currents obtained from direct

measurements in canine atrial myocytes, and compare the behavior of model APs to experimental measurements of rate-dependent, regionally-determined, and electrically-remodeled APs in dog atrium.

2.2 Model Description

The cell membrane is modeled as a capacitor connected in parallel with variable resistances (ion channels) and batteries (driving forces). The rate of change in the transmembrane potential, V, is given by

$$\frac{dV}{dt} = \frac{-(I_{ion} + I_{stim})}{C_m} \tag{2.1}$$

where I_{ion} and I_{st} are the total transmembrane ionic current and stimulus current, respectively, and C_m is the total membrane capacitance. The total transmembrane ionic current is given by

$$\begin{aligned} I_{ion} &= I_{Na} + I_{K1} + I_{to} + I_{Kur,d} + I_{Kr} + I_{Ks} + I_{Ca} + I_{Cl,Ca} + I_{p,Ca} \\ &\quad + I_{NaCa} + I_{NaK} + I_{b,Na} + I_{b,Ca} \end{aligned} \tag{2.2}$$

Intracellular concentrations of Na^+, K^+, Ca^{2+}, and Cl^- are monitored. Extracellular concentrations are kept constant throughout. Figure 2.1* is a schematic representation of the canine atrial myocyte used in the model, which includes membrane currents, pumps and exchangers. The intracellular space also includes network (Ca^{2+}-uptake) and

*Figures and captions are located at the end of chapter 2 on page 46.

junctional (Ca^{2+}-release) compartments of the sarcoplasmic reticulum (NSR and JSR, respectively) that play a role in the intracellular handling of Ca^{2+}.

We integrate equation 1 using a modified Euler method with a fixed time step of $\Delta t = 0.005\ ms$. This ensures that the largest change in transmembrane potential over a single time iteration does not exceed 0.25 mV [63]. All simulations were performed using double precision arithmetic. The full system of equations and constants are given in the appendices.

2.2.1 Membrane Currents

Fast Na^+ current. The model implements I_{Na} as a modification of the Ebihara-Johnson model [15] proposed by Luo and Rudy [41], and is given by

$$I_{Na} = g_{Na} \cdot m^3 \cdot h \cdot j \ (V - E_{Na}) \ . \tag{2.3}$$

Transient outward K^+ current. We formulate I_{to} based on results obtained from our laboratory in isolated canine atrial myocytes [71, 73]. Activation and inactivation of I_{to} are rapid. Figure 2.2A shows steady state values for activation (solid line) and inactivation (dashed line) used in the model. The experimental values (symbols) from Yue et al [71] were fit using a Levenberg-Marquardt nonlinear least squares algorithm [42]. Figure 2.2B shows the corresponding time constants. The activation time constant is bell-shaped, with a maximum of 5.9 ms at -27 mV. Since experimental data for activation

kinetics (τ_{oa}) are unavailable for potentials below -10 mV in dog, we implement the formulation from the human atrial AP model [11] and fit the data from canine cells. The inactivation time constant changes very little at depolarized potentials positive to 10 mV. Experimental values for onset and removal of inactivation are represented by open and filled circles, respectively. The current is given by

$$I_{to} = g_{to} \cdot o_a^3 \cdot o_i \ (V - E_K) \ . \tag{2.4}$$

Figure 2.2C shows the simulated response of I_{to} to a voltage clamp pulse protocol (inset). The maximal I_{to} conductance, g_{to}, was adjusted to obtain current amplitudes that agreed with experimental observations. The peak current-voltage relation (figure 2.2D) obtained by the model (solid line) shows excellent agreement with values reported by Yue et al [71] (circles).

Dog ultrarapid delayed rectifier K^+ current. The model implements $I_{Kur,d}$ based on results obtained from our laboratory in isolated canine and human atrial myocytes [72, 65]. The current is given by

$$I_{Kur,d} = g_{Kur,d} \cdot u_a^3 \cdot u_i \ (V - E_K) \ , \tag{2.5}$$

$$g_{Kur,d} = 0.009 + \frac{0.082}{1 + \exp\left[\dfrac{V + 11}{-16}\right]} \ , \tag{2.6}$$

where $g_{Kur,d}$ is the maximal conductance. Figures 2.3A and 2.3B show steady state values and time constants for activation and inactivation of $I_{Kur,d}$. The activation time constant shown in figure 2.3B (dashed line) is fit to values reported by Yue et al [72] (triangles).

Inactivation of $I_{Kur,d}$ is very slow. In the absence of canine-specific measurements for $I_{Kur,d}$ inactivation at 37 °C, we have used the inactivation steady steady state and time constant for human atrial myocytes reported by our laboratory [65] and used previously in our human atrial AP model [11]. Figure 2.3C shows $I_{Kur,d}$ elicited from a pulse protocol. The peak I-V relationship in figure 2.3D shows good agreement with data from Yue et al [72] (circles).

Rapid and slow K^+ delayed rectifier current components. The model implements the rapid and slow components of the classical delayed rectifier, I_{Kr} and I_{Ks}, based on data from isolated canine atrial myocytes obtained in our laboratory [71, 73]. The currents are given by

$$I_{Kr} = g_{Kr} \cdot x_r \left(0.07 + \frac{0.58}{1 + \exp[(V + 15)/22.4]}\right) (V - E_K) \ , \tag{2.7}$$

$$I_{Ks} = g_{Ks} \cdot x_s^2 \ (V - E_K) \ . \tag{2.8}$$

Both components have only a single activation gate, shown in figure 2.4A. Experimental values for steady-state activation of I_{Kr} and I_{Ks} are from Li et al [34]. Figure 2.4B shows the activation time constants determined from fits of unpublished data obtained in our laboratory. The experimental data shows activation (open symbols) and deactivation (filled symbols) for both I_{Kr} and I_{Ks}. Panels C and D show delayed rectifier currents elicited in the model by the pulse protocol shown in the inset. Panels E and F show the peak I-V relationships obtained by the model (lines) and from Li et al (symbols) [34].

Inward rectifier K^+ current. The model follows the formulation of I_{K1} used previously in our human AP model [11]. Maximal conductance, g_{K1}, is adjusted to obtain a peak I-V relation that corresponds to results obtained from our laboratory [73]. The current is given by

$$I_{K1} = \frac{g_{K1}\,(V - E_K)}{1 + \exp[0.07(V + 80)]}\ . \tag{2.9}$$

Ca^{2+} current. We base our formulation of the Ca^{2+} current on experimental data obtained in our laboratory [73] and previous AP models [11, 41]. The current is given by

$$I_{Ca} = g_{Ca} \cdot d \cdot f \cdot f_{Ca}\ (V - 65)\ . \tag{2.10}$$

The formulation includes voltage-dependent activation (d), and voltage- and Ca^{2+}-dependent inactivation (f and f_{Ca}). The Nernst relationship (equation A.12 in appendix A) for calcium gives an equilibrium potential between 100 and 130 mV, which does not correspond to experimental observations of I_{Ca} reversal [17, 34, 73]. The reversal potential for I_{Ca} is therefore fixed at 65 mV. The steady state activation and inactivation variables (figure 2.5A) and the time constant for voltage-dependent inactivation (τ_f in figure 2.5B) are fit to values obtained from isolated canine atrial myocytes as reported by Yue et al [73]. In the absence of reported activation time constants specific to canine atria, we have adopted the formulation used by Luo and Rudy [41]. Figure 2.5C shows the steady-state Ca^{2+}-dependent inactivation gate for I_{Ca}; this variable differs from previous models [11] in that inactivation saturates at values of $[Ca^{2+}]_i$ above 0.35 μM, and the concentration dependence has a steeper slope. Figure 2.5E shows I_{Ca} resulting from a pulse protocol.

The peak I-V relationship obtained by the model (panel F) is U-shaped and reverses around +65 mV. The peak I-V relation for I_{Ca} in the model captures the key features reported by Yue et al [73] (figure 2.5F). Calcium transients elicited at different rates are shown in figure 2.5D.

Ca^{2+}-activated Cl^- current. The detailed mechanism of $I_{Cl,Ca}$ activation remains poorly understood, although direct activation by free cytoplasmic Ca^{2+} appears central. Several factors exert a degree of control on $I_{Cl,Ca}$ including channel density, colocalization with sarcolemmal Ca^{2+} channels, Ca^{2+} load in the sarcoplasmic reticulum (SR), and calcium-induced calcium release [10]. In the model, activation of $I_{Cl,Ca}$ is initiated by Ca^{2+} flux into the cell, aiming to represent the increase in $[Ca^{2+}]_i$ in a localized region between the closely coupled sarcolemmal I_{Ca} and the Ca^{2+}-release channels of the SR [33, 75]. The current is given by

$$I_{Cl,Ca} = g_{Cl,Ca} \cdot q_{Ca} \, (V - E_{Cl}) \, . \tag{2.11}$$

Figure 2.6A shows the Ca^{2+}-dependent activation of the current. In response to depolarizing pulses, $I_{Cl,Ca}$ is a transient outward current (figure 2.6B) that decays fully within 20 ms of the onset of depolarization. The peak I-V relation (figure 2.6C) is similar to experimental values (circles in figure) reported by Yue et al [73].

Na^+-K^+ pump current. We implement the Na^+-K^+ pump as in the Luo and Rudy model [41]. The current is given by

$$I_{NaK} = I_{NaK(max)} \cdot f_{NaK} \, \frac{1}{1 + (K_{m,Na(i)}/[Na^+]_i)^{1.5}} \cdot \frac{[K^+]_o}{[K^+]_o + K_{m,K(o)}} \tag{2.12}$$

The maximal current, $I_{NaK(max)}$, is adjusted to maintain stable intracellular ion concentrations at rest.

Na^+/Ca^{2+} exchanger current. We implement the exchanger current following the formulation of Luo and Rudy [41]. The exchanger current is given by

$$I_{NaCa} = I_{NaCa(max)} \cdot \frac{[Na^+]_i^3[Ca^{2+}]_o \exp[\gamma\frac{VF}{RT}] - [Na^+]_o^3[Ca^{2+}]_i \exp[(\gamma-1)\frac{VF}{RT}]}{(K_{m,Na}^3 + [Na^+]_o^3)(K_{m,Ca} + [Ca^{2+}]_o)\left(1 + k_{sat}\exp[(\gamma-1)\frac{VF}{RT}]\right)} \quad (2.13)$$

Background Na^+ and Ca^{2+} currents. The amplitudes of the background currents are adjusted in conjunction with I_{NaK} to maintain stable intracellular concentrations of Na^+, K^+ and Ca^{2+} at rest. The currents are given by

$$I_{b,Na} = g_{b,Na}\ (V - E_{Na})\ , \quad (2.14)$$

$$I_{b,Ca} = g_{b,Ca}\ (V - E_{Ca})\ . \quad (2.15)$$

Ca^{2+} pump current. We include a sarcolemmal Ca^{2+} pump current which assists in $[Ca^{2+}]_i$ regulation. Formulation of this pump current follows Luo and Rudy [41] and is given by

$$I_{p,Ca} = I_{p,Ca(max)}\ \frac{[Ca^{2+}]_i}{0.0005 + [Ca^{2+}]_i}\ . \quad (2.16)$$

SR Ca^{2+} handling. The SR serves as an intracellular storage compartment for Ca^{2+}. Calcium is released from, and sequestered to, the SR to regulate intracellular Ca^{2+} homeostasis. We implement this Ca^{2+} handling using the two compartment model of Luo and Rudy [41] with the modification proposed by Friedman [21]. A network SR (NSR)

compartment subserves Ca^{2+}-uptake, while a junctional compartment (JSR) governs release. The uptake current, I_{up}, moves Ca^{2+} from the intracellular space to the NSR, while I_{rel} releases Ca^{2+} from the JSR to the myoplasm. We implement a transfer current, I_{tr}, to quantify the movement of Ca^{2+} from the NSR to the JSR. These currents are given by

$$I_{up} = \frac{I_{up(max)}}{1 + (K_{up}/[Ca^{2+}]_i)} , \tag{2.17}$$

$$I_{tr} = \frac{[Ca^{2+}]_{up} - [Ca^{2+}]_{rel}}{\tau_{tr}} , \tag{2.18}$$

$$I_{rel} = k_{rel} \cdot u^2 \cdot v \cdot w \ \left([Ca^{2+}]_{rel} - [Ca^{2+}]_i\right) . \tag{2.19}$$

Calcium release from the JSR is induced by Ca^{2+} flux into the myoplasm with emphasis on the close coupling between sarcolemmal I_{Ca}-channels and I_{rel}-channels of the SR. The release current is thus a transient Ca^{2+}-flux with a negative feedback that contributes to its rapid inactivation following a brief opening. Activation and inactivation gating for I_{rel} are implemented as described previously in our human atrial AP model [11].

Myoplasmic and SR Ca^{2+} buffers. Ca^{2+} buffering is mediated by calmodulin and troponin in the myoplasm, and by calsequestrin in the SR release compartment (JSR). Throughout our simulations, buffers are considered at equilibrium. Separation of Ca^{2+} into free and buffer-bound concentrations is modeled as an instantaneous process. Buffer concentrations and binding constants (given in appendices) are from Luo and Rudy [41] and Rasmusson et al [55].

2.3 Results

2.3.1 Canine AP Model

The canine atrial AP model has a stable membrane potential of about -83 mV at rest and stable intracellular ion concentrations of $[Na^+]_i$ = 11.8 mM, $[K^+]_i$ = 138.4 mM, $[Ca^{2+}]_i$ = 0.10 μM, and $[Cl^-]_i$ = 29.3 mM. The resting membrane potential is maintained by I_{K1}, I_{NaCa}, I_{NaK}, and the background currents ($I_{b,Na}$ and $I_{b,Ca}$). Upon stimulation of a model AP, the membrane potential depolarizes to about +40 mV, exhibits a rapid initial repolarization phase followed by a plateau near -15 mV and a final repolarization phase, yielding an action potential duration (APD_{95}) of 201 ms at 1 Hz. Figure 2.7 shows the action potential (upper left panel) and the ionic currents that underlie its morphology. The time course of the model AP is superimposed (dotted line) over each ionic current to facilitate comparisons and to indicate the portion of the AP during which each current is present. The calcium transient is shown in the lower right panel.

The fast, inward I_{Na} is responsible for the rapid upstroke of the AP. Rapid inactivation of I_{Na} and the onset of I_{to}, $I_{Kur,d}$, and $I_{Cl,Ca}$ mediate the initial repolarization phase which lasts about 10 ms following AP initiation. The initial decay of these rapid repolarizing currents is followed by a plateau phase which represents a balance between I_{Ca} and $I_{Kur,d}$. The delayed rectifiers, I_{Kr} and I_{Ks}, dominate during the terminal stages of the plateau, and together with I_{K1} govern the final repolarization phase.

2.3.2 Variability of AP Morphology

There exists a wide variation of canine atrial AP morphologies that may be observed experimentally [17]. This variation persists within individual hearts and even within myocytes that might be closely localized in the same atrial region. The likely explanation for this range of morphologies is a variation in ionic conductances among myocytes [17]. One advantage of a mathematical model over experimental preparations is the ability to investigate the effects of specific variation in individual ionic currents on the AP. Using the model, we examined the relationship between AP morphology and maximal conductances of individual ionic currents (including I_{to}, $I_{Kur,d}$, I_{Kr}, I_{K1}, $I_{Cl,Ca}$, and I_{Ca}) by varying the maximal conductance from 10 to 300% of the standard value in the model. Figure 2.8 summarizes these results. Each AP waveform represents the tenth AP following pacing from rest at 1 Hz. The control model AP is shown in each panel in bold. A 90% decrease in the conductance of a specified channel is represented by a dotted line; a 300% increase in conductance, by a dashed line.

Action potential duration increases when the conductance of repolarizing currents decreases (figure 2.8 A-E); however, the nature and degree of prolongation is different for each ionic current. For I_{to}, APD prolongation saturates with decreasing conductance. As I_{to} conductance decreases from 75% to 10%, the rate of initial repolarization is slowed slightly and the plateau is raised progressively; however, the more positive plateau potential activates more I_K, accelerating phase 3 repolarization and leaving total APD

relatively unaffected. Increased plateau potential without an accompanying increase in APD from I_{to} blockade is observed experimentally in isolated canine myocytes using 2 mM 4-aminopyridine [71]. For $I_{Kur,d}$, the plateau of the AP is raised as conductance decreases, accentuating the spike and dome morphology of the AP, and prolonging APD. Conversely for both I_{to} and $I_{Kur,d}$, an increase in conductance progressively shortens the APD and yields APs that are triangular in morphology.

The late repolarization phase is strongly affected by I_{Kr}, and the AP response to changing this current reflects this property. Changes in I_{Kr} conductance have no effect on the initial phase of repolarization or the early part of the plateau. The effect of I_{Kr} modulation is manifest towards the end of the plateau and throughout the late repolarization phase with an APD response as expected – decreased I_{Kr} prolongs APD, whereas increased I_{Kr} shortens APD. Selective blockade of I_{Kr} can be performed experimentally with E-4031, and prolongs APD in a manner consistent with our model [71]. Activation of I_{Ks} is almost three times slower than I_{Kr} in our model (fig 2.4). As a result, peak I_{Ks} is more than ten times smaller than I_{Kr} over the course of an AP at 1 Hz (fig. 2.7). Thus, changes in I_{Ks} conductance, from 90% block to 300% increase, did not alter APD_{95} by more than 5 ms (not shown).

For I_{K1}, a decrease in conductance makes the resting membrane potential progressively more positive and prolongs the APD. Increased I_{K1} conductance has little effect on resting potential but shortens APD. Significant depolarization begins when I_{K1} is reduced by 50% from the baseline level. $I_{Cl,Ca}$ is a transient outward current that activates

	Frequency (Hz)					
	0.1	1.0	2.0	3.0	4.0	5.0
APD_{90} (ms)	226	179	147	131	122	116
APD_{95} (ms)	252	201	164	147	137	131
APA (mV)	119	119	119	118	118	116
APO (mV)	35.5	35.4	35.9	35.5	36.1	34.8
EDP (mV)	-83.5	-83.6	-83.1	-82.5	-81.9	-81.2
$\dot{V}max$ (V/s)	230	230	230	226	225	215

Table 2.1: Rate-adaptation of AP characteristics. APD_{95} and APD_{90}, time for 95% and 90% repolarization; APA, AP amplitude; APO, AP overshoot above 0 mV; EDP, end-diastolic potential immediately prior to AP; $\dot{V}max$, maximal upstroke velocity.

during the initial repolarization phase of the AP. The contribution of $I_{Cl,Ca}$ to membrane repolarization during this phase is about 5% of the combined effects of I_{to} and $I_{Kur,d}$; thus, a 90 % reduction in conductance yielded only a 5 ms increase in APD_{95}, while a 300 % increase in conductance decreased APD_{95} by only 10 ms (panel E). The effect on AP morphology of varying I_{Ca} was the opposite for that of $I_{Kur,d}$, which is expected since the AP plateau is sustained via a balance between these two currents. A reduction in I_{Ca} conductance progressively lowers the plateau and shortens APD; while an increase in conductance raises the plateau, accentuates the spike and dome morphology, and prolongs APD. Nifedipine block (5 μM) of I_{Ca} in isolated canine atrial myocytes shortened APD and produced triangular APs, consistent with our model [71].

2.3.3 APD Adaptation to Rate

The adaptation of APD and refractoriness to changes in rate is an important physiological property and plays a significant role in the generation and maintenance of atrial arrhythmias [3, 69, 73]. Table 2.1 lists properties of the model APs and their values at rates between 0.1 and 5.0 Hz after 10 seconds of pacing. As frequency increases from 0.1 Hz to 5.0 Hz, APD_{95} decreases from 252 ms to 131 ms. End-diastolic potential (EDP), AP amplitude (APA) and overshoot (APO) are little affected. Figure 2.9 compares model APs (left) with experimental recordings (right) at 0.1, 1.0, and 2.0 Hz. The morphology of model APs generally agree with experimental recordings. At the slower pacing frequencies, both model and experimental APs exhibit a distinct plateau, and become more triangular as the frequency increases.

To identify the mechanism of rate-adaptation in the model, we utilized a simulation protocol in which we isolated individual variables and examined their effect on AP morphology. Using recordings of APs paced at 4 Hz, we selected variables suspected of contributing to APD-shortening. We then used these selected variables as initial conditions prior to an impulse generated at 1 Hz. The resultant alteration in morphology of the subsequent AP can then be attributed to the isolated variable(s). In this way, we investigated the roles of I_{Kr}- and I_{Ks}-activation, voltage-dependent inactivation of I_{Ca}, and rate-dependent changes in intracellular concentrations of calcium. Figure 2.10 shows the results of this simulation protocol. Control APs at 1 Hz and 4 Hz are shown as thick

dashed and dotted lines, respectively. The three thin lines with symbols represent the AP obtained following the substitution of the indicated variable(s). When the activation variables for I_{Kr} and I_{Ks} at 4 Hz are substituted into the AP at 1 Hz (square symbol), there is neither significant change in AP morphology nor APD shortening. Substitution of the voltage-dependent inactivation variable for I_{Ca} (denoted f in equation 2.10, circles in figure 2.10) produces plateau depression, and accounts for over 50 % of the observed APD shortening. The remaining APD shortening observed between APs at 1 Hz and 4 Hz is achieved by substitution of the values for intracellular concentrations of calcium (both in the myoplasm and sarcoplasmic reticulum) in addition to voltage-dependent inactivation of I_{Ca} (triangles).

Unlike the human AP model [11], I_K does not play a direct role in atrial AP rate-adaptation over 1 - 4 Hz in the present model. The positioning (membrane potential) of the AP plateau determines the amount of I_K recruitment which affects late repolarization; the positioning of the plateau phase is determined largely by voltage- and calcium-dependent inactivation of I_{Ca} in the model. In addition to calcium-dependent inactivation of I_{Ca}, the calcium transient also determines I_{NaCa} over the course of the AP. Calcium release from the SR, bulk intracellular [Ca^{2+}], and voltage-dependent inactivation of I_{Ca} are the predominant determinants of AP rate-adaptation in the present model.

	PM	CT	APG	AVR
I_{Ca}	1.0	1.58	1.06	0.67
I_{to}	1.0	1.0	0.53	1.0
I_{Kr}	1.0	1.0	1.0	1.63
I_{Ks}	1.0	1.0	1.0	1.0
$I_{Kur,d}$	1.0	1.0	1.0	1.0
I_{K1}	1.0	1.0	1.0	1.0

Table 2.2: Regional variations in ionic current density from atrial myocytes in the crista terminalis (CT), appendage (APG), and AV ring region (AVR) normalized to cells from pectinate muscle (PM).

2.3.4 Regional Heterogeneity

Atrial AP heterogeneity plays an important role in the generation and maintenance of atrial reentrant arrhythmias [16, 49]. Feng et al used whole-cell voltage clamp experiments to examine canine atrial myocytes from four right atrial regions: the appendage, crista terminalis, pectinate muscle, and the AV ring region [17]. They demonstrated regional variation in the densities of I_{Ca}, I_{to}, and I_{Kr} that were associated with regional variations in AP morphology. Other currents (I_{K1}, I_{Ks}, and $I_{Kur,d}$) did not show regional variation, and the voltage- and time-dependence of currents did not vary among regions, suggesting that regional differences resided in the relative current amplitudes and not in other biophysical properties. The ionic current profiles from each region (table 2.2) were implemented in the model to determine whether the differences noted were significant to account for the regional AP morphology variations.

Figure 2.11 shows the APs obtained by modifying currents in the model according

APD_{95} (ms)	PM	CT	APG	AVR
model	188	231	205	142
experiment	190	270	180	160

Table 2.3: APD_{95} in cells from different regions of canine right atrium in model and experiment.

to reported measurements of ionic currents in each region (left column) and digitally averaged APs obtained from all APs recorded experimentally in the corresponding regions by Feng *et al.* [17] (right column). AP morphology in the model showed good qualitative agreement with the averaged AP waveforms obtained experimentally from the corresponding regions. The basic model AP had the closest morphological resemblance to pectinate myocyte APs (upper panel), as well as good concordance in APD_{95} measurement (table 2.3). Experimental APs from the crista terminalis (CT) showed a spike and dome morphology and the longest APD of all the regions, in general agreement with the model. Appendage (APG) myocytes displayed a positive plateau and rectangular morphology. The model APs had similar qualitative features, with a less positive plateau potential; however, recordings from this region showed the largest variability in AP morphology [17]. Myocytes from the AV ring region (AVR) had a triangular AP morphology and short APD, again similar to model simulations. Similar to experimental observations, model APs were longest in the CT, shortest in the AVR, and intermediate in the PM and APG regions. APs in CT and AVR were, however, slightly shorter in the model compared to experimental observations (table 2.3).

2.3.5 Ionic Remodeling in AF

Rapid atrial activation provides a substrate for AF [23] that may be exacerbated by increased regional heterogeneity. Yue *et al.* [73] utilized a rapid pacing model of AF in dogs to investigate the ionic mechanism associated with electrical remodeling. Dogs were subjected to up to 42 days of atrial pacing at 400 beats per minute, after which atrial myocytes were isolated and examined. The isolated myocytes were grouped according to duration of rapid pacing: no pacing (control group, denoted P0), one day (P1), seven days (P7), and 42 days (P42) of rapid pacing. Electrophysiologic examination of these myocytes revealed that I_{Ca} and I_{to} current densities decreased progressively without any concomitant change in kinetics or voltage-dependence. No other ionic currents were affected, and time- and voltage-dependent properties of I_{Ca} and I_{to} were unaltered by rapid pacing. Table 2.4 summarizes the mean reduction of I_{Ca} and I_{to} during rapid atrial pacing determined experimentally (as values normalized to those of the control group). These values were implemented in the model to simulate the effect of atrial tachycardia-induced ionic remodeling.

Figure 2.12 shows the resulting APs for the four groups in the model (left column) at 0.1 Hz and 2.0 Hz and corresponding experimental recordings from representative myocytes (right column). When the reductions in I_{Ca} and I_{to} reported by Yue et al

	I_{Ca}	I_{to}
P0	1.0	1.0
P1	0.69	0.73
P7	0.48	0.46
P42	0.31	0.35

Table 2.4: Reduction of I_{Ca} and I_{to} during rapid atrial pacing in four groups of dogs: P0 - control; P1 - one day of rapid pacing; P7 - seven days of rapid pacing; and P42 - 42 days of rapid pacing. Mean current density in each group is normalized to that of P0 dogs.

are simulated, the model shows APD_{95} shortening and loss of rate adaptation that is qualitatively similar to experimental observations. Quantitatively, APD abbreviation was more affected in experiments than predicted by the model for the ionic changes reported. Adaptation of APD to changes in rate was essentially abolished in myocytes of dogs subjected to rapid atrial pacing for 42 days, but still occurred in the model. The implementation of additional attenuation (to 10% of control values) in I_{Ca} conductance in model P42 simulations (inset) reproduced the experimentally observed loss of rate-adaptation.

2.4 Discussion

We have developed a mathematical model of the canine atrial AP. The model produces APs that are consistent with experimental observations under a variety of conditions, and permits critical analysis of the mechanisms and interactions of ionic currents that

underlie AP changes in different situations.

2.4.1 Behavior of the Model AP

Variability of AP morphology. Action potentials measured in isolated canine myocytes exhibit a wide range of morphologies. This propensity for a wide range of AP morphologies exists even among cells isolated from small myocardial regions within an individual. Wang et al [66] identified three principal AP morphologies in human atrial myocytes. Type 1 APs had a spike-and-dome waveform; type 2, an elevated, level plateau phase; and type 3, a triangular AP with little to no plateau region. On the basis of patch-clamp techniques, they determined that the variable AP morphologies corresponded with differences in the relative amplitudes of I_{to} and the delayed rectifier current, I_K. More recently, Feng et al [17] suggested an ionic basis for regional AP heterogeneity in the canine right atrium. Our canine AP model supports the view that an ionic substrate underlies the variability of AP morphologies observed in canine atria. Action potential morphology is sensitive to ion conductance in the model (figure 2.8), particularly during the plateau phase of the AP.

Individual ionic currents exerted unique effects on AP morphology. Reduction of I_{to} conductance prolonged APD in a saturating manner, while augmentation of this current greatly shortened APD. The effect of modulating each ionic current highlighted the phase of the AP cycle in which it played a prominent role. The positioning of the

plateau and the presence or absence of a spike and dome was dependent on $I_{Kur,d}$ and I_{Ca} conductance, while the end-diastolic potential and the rate of final repolarization were controlled primarily by I_{K1}.

Rate-adaptation of the model AP. Normal atrial myocytes exhibit substantial rate-dependent modulation of refractoriness and APD. Loss of rate-adaptation has been linked to electrical remodeling due to AF [46], and to vulnerability to AF induction in man [3]. Rate-adaptation of the AP in the model is consistent with experimental findings – a reduction in basic cycle length is associated with an abbreviation of the plateau and a decrease in its slope. The central role of I_{Ca} changes in the rate-dependent AP behavior of the model is consistent with experimental observations [73].

2.4.2 AP Model Applications

Regional heterogeneity. Heterogeneity in atrial refractoriness plays an important role in AF maintenance [16]. Discrete differences in AP morphology and APD among cells from different regions of atrial tissue can contribute to the generation of localized reentrant circuits [49]. The reproduction of regional differences in ionic conductances, as reported by Feng et al [17], produced model APs with APD_{95} and morphologies closely resembling those observed experimentally in the corresponding region (figure 2.11). Our model thus supports an ionic substrate as the basis for regional AP heterogeneity and constitutes

the first quantitative effort of which we are aware to determine whether regional variations recorded in ionic currents can account for observed AP differences. Furthermore, the agreement in morphology and time course of model APs with mean experimental recordings from four distinct regions of the canine right atria emphasizes the versatility and practicality of this model.

AF-induced electrical remodeling. Rapid pacing in canine atria has been shown to decrease APD and adaptation to changes in rate. These changes are associated with progressive reductions in I_{Ca} and I_{to} [73]. As shown in figure 2.12, APD_{95} decreases with increased pacing in isolated canine atrial myocytes (right), as well as in the model (left) when associated reductions in I_{Ca} and I_{to} density are reproduced. The decrease in APD_{95} in the model is not as prominent as that observed in myocytes, and the loss of rate adaptation to pacing frequency is not as striking in the model as in experiments. These findings may suggest that the observed changes in I_{Ca} and I_{to} are, by themselves, insufficient to account for the rapid pacing-induced changes in AP morphology. Rapid pacing studies in dogs [25] and goats [59, 60] have suggested that electrical remodeling of the atria is mediated by intracellular calcium overload. Thus, other ion transport processes, including the Na^+/Ca^{2+} exchanger [53], $Na^+ - K^+$ pump, or proton pump, which have not been studied experimentally in pacing-induced remodeling, may be involved. Furthermore, the experimental analysis of isolated canine atrial myocytes was conducted using 10 mM intracellular EGTA, a strong calcium buffer, while model

simulations of the ionic changes associated with AF-induced electrical remodeling are performed using intact calcium handling processes. Additional regulatory changes may occur. For example, inefficient coupling between sarcolemmal I_{Ca} and SR Ca^{2+} release is associated with hypertrophy in rat ventricular myocytes [26, 56]. To our knowledge, this sort of reduced coupling has not yet been examined in AF-induced remodeled canine atrial myocytes. Alternatively, the lack of full agreement with experimental findings may be due to inadequate expression by the model of changes in ionic processes at rapid rates.

2.4.3 Comparison With Other AP Models

Previous atrial action potential models have been published for bullfrog, rabbit, and human atrial myocytes. To our knowledge, this is the first canine-specific atrial AP model. In 1990 Rasmusson et al [55] described a mathematical model of the bullfrog atrial cell. This model grouped the voltage- and time-dependent repolarizing K^+ currents into a single I_K. The model (monophasic) AP displayed a rounded peak and lacked a distinct initial repolarization phase (phase 1). The upstroke of their model AP consisted of a rapid phase and a secondary slow phase as there was no I_{to}- or I_{Kur}-like current to mediate initial repolarization. In addition, that model did not include a SR component for intracellular uptake or release of Ca^{2+}.

Lindblad et al [39] described a mathematical model of the rabbit atrial cell that incorporated intracellular Ca^{2+} handling by the SR and provided a more complete formulation

of repolarizing K^+ currents including a transient outward current (I_t) and rapid and slow components of the delayed rectifier current. Unlike the present canine atrial AP model I_{Ca} inactivation was not modulated by intracellular Ca^{2+}. Adaptation of AP morphology to changes in rate was very sensitive in the Lindblad model for frequencies between 0.2 and 3 Hz. This sensitivity was attributed primarily to inactivation of I_{to} and its role in initial repolarization (phase 1). At 3 Hz, their model AP displayed an elevated plateau potential of about 30 mV, which decreased to about -35 mV when the cell was paced at 0.2 Hz. Although their model reproduced the rabbit atrial AP well, species differences limit its applicability to the dog. These differences are especially evident in the transient outward and delayed rectifier currents.

More recently, models of the human atrial AP have been published by Nygren et al [52] and Courtemanche, Ramirez and Nattel [11] (here referred to as the CRN model). Both models included descriptions of similar ionic currents. Human atrial myocytes display a longer APD_{90} than in the dog (66% longer in the CRN model than in the present model). Comparison of the underlying currents in this and the CRN model reveals that I_{Ca} activates and inactivates faster in the canine model than in the human model. This abbreviates both the plateau potential and duration, and consequently shortens APD, in agreement with observed differences between human and canine atrial APDs. The reduced plateau potential in the present canine model also results in less contribution to repolarization from the delayed rectifier currents. Late repolarization in the canine model has a larger I_{K1} contribution than in the CRN model.

2.4.4 Potential Limitations

Experimental investigations of ion channels often introduce an amplitude bias that stems from the selection of cells with large currents and cell viability. That is, small currents are likely to be considered inadequate for study and thus not represented in presentation of experimental data. As a result, it is often necessary in formulating an AP model, to scale the current densities in order to obtain appropriate AP properties. In the present model, I_{Ca} was the only current whose density needed adjustment. I_{Ca} density in the model was 33% of mean values determined experimentally. Scaling of ionic currents has been used extensively in previous AP models [11, 31, 52].

Our model includes a transient outward Ca-activated chloride current, $I_{Cl,Ca}$, that is commonly observed in isolated canine myocytes. The mechanism of activation for this current is not yet fully understood. In the model, we formulate this current using an arbitrary calcium-dependent activation scheme that closely reproduces the observed peak I-V relationship (fig 2.6). There is evidence from rapid-paced dogs that reductions in sarcolemmal I_{Ca} are not accompanied by alterations in $I_{Cl,Ca}$ [73]. This suggests that $I_{Cl,Ca}$ is regulated by additional factors that are not considered in the present model. Furthermore, it is not clear how intracellular chloride homeostasis is maintained in the cell. In the present model, we do not include any regulatory mechanism to counterbalance the outward movement of Cl^- via $I_{Cl,Ca}$. Within the framework of the AP, however, $I_{Cl,Ca}$

is of limited importance (figures 2.7 and 2.8E), and the accumulation of intracellular Cl^- during activity at 1 Hz occurs very slowly, at a rate of about 1.6 mM/hr (6.43 mM in 4 hours).

The delayed rectifier currents, I_{Kr} and I_{Ks}, play an integral role in cellular repolarization. Yet sensitivity analysis of individual ionic currents reveals that alterations to I_{Ks} conductance produce no significant changes in APD or AP morphology in the model. Delayed rectifier currents are particularly sensitive to damage in the cell isolation process [71], so it is possible that the limited role of I_{Ks} in repolarization of model APs is due to an under-representation of the current's amplitude in experimental observations. In addition, a variety of manipulations (such as inorganic or organic I_{Ca} blockers, dialysis of cellular macromolecules, and conditions to suppress other potentially contaminating currents) may alter the density or kinetics of experimentally recorded I_{Kr} and I_{Ks}. Therefore, the suggestion of the model that changes in I_{Kr} and I_{Ks} do not play a role in AP rate adaptation should be interpreted with caution. Further experimental and theoretical work will be needed to clarify better the properties of I_{Kr} and I_{Ks} under physiological conditions and their role in canine atrial AP rate adaptation. Taken at face value, the lack of significant influence of the delayed rectifiers on AP morphology may suggest an important discrepancy between human and canine atrial AP properties.

2.4.5 Potential Significance

Canine and human atrial myocytes share a variety of ionic current properties [73], making canine models useful for understanding human atrial arrhythmias. The present model provides a useful tool for analyzing the role of ionic currents in canine atrial APs and arrhythmia mechanisms. Our model shows that interactions of currents play an important role in determining the properties of the action potential. Modulation of specific current conductances can have secondary effects on other currents via voltage-dependence of channel properties (figure 2.8). This is as important consideration when designing drugs that may alter ion channel properties.

Atrial fibrillation is the most frequently encountered sustained arrhythmia in clinical practice. Key features associated with AF include loss of rate-adaptation [5] and AP heterogeneity [49]. Our model reproduces adaptation to changes in rate that is similar to observed phenomena (figure 2.9), and thereby gives potential insights into their mechanisms. These investigations point to SR-loading, intracellular $[Ca^{2+}]$, and I_{Ca} voltage-dependent inactivation as important mediators of rate adaptation (figure 2.10), and support the role of an ionic substrate for regional AP heterogeneity as suggested by Feng et al [17].

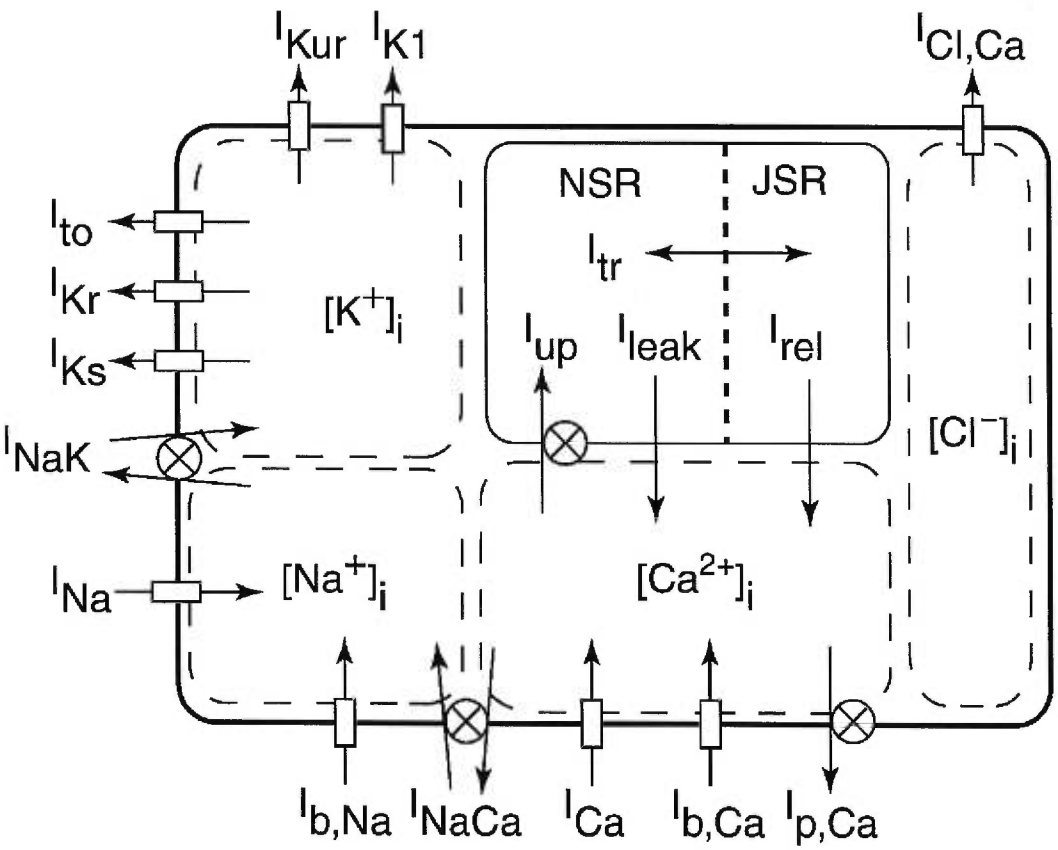

Figure 2.1: Schematic representation of the canine atrial model myocyte. Dashed intracellular compartments indicate the intracellular pools of ion species. The ion concentration in each pool is affected by ionic currents, pumps, and exchangers. Rectangular boxes indicate sarcolemmal ion currents. Pumps and exchangers are indicated by crossed circles. The SR is divided into two compartments: the Ca^{2+} release compartment or junctional SR (JSR), and the Ca^{2+} uptake compartment or network SR (NSR).

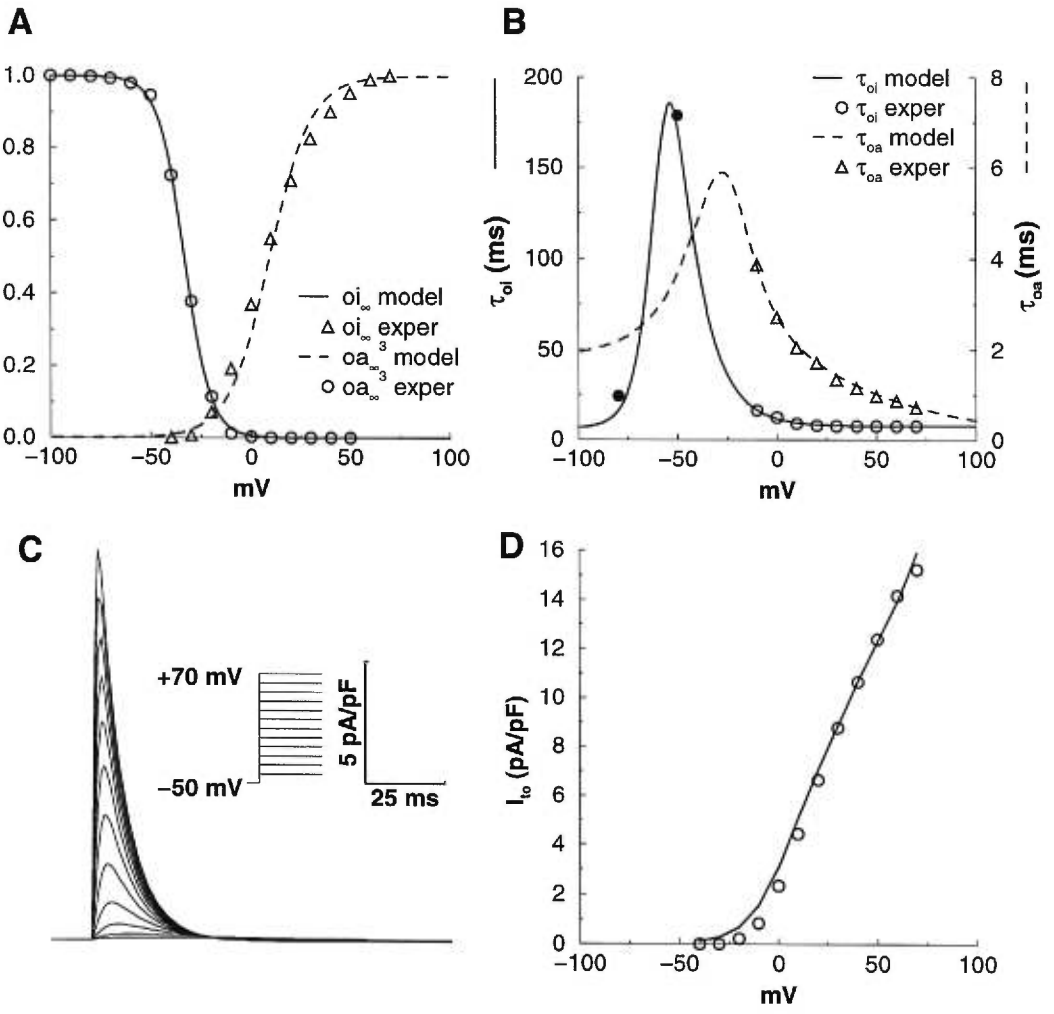

Figure 2.2: Transient outward K^+ current, I_{to}. (A) Activation (dashed line) and inactivation (solid line) steady state values and corresponding experimental data. (B) Time constant values for activation (dashed line) and inactivation (solid line) and corresponding experimental data (symbols). The filled circles represent removal of inactivation determined experimentally. (C) I_{to} response to voltage steps in the model (pulse protocol in inset). (D) Peak $I - V$ relation for model (line) and in experiments (circles).

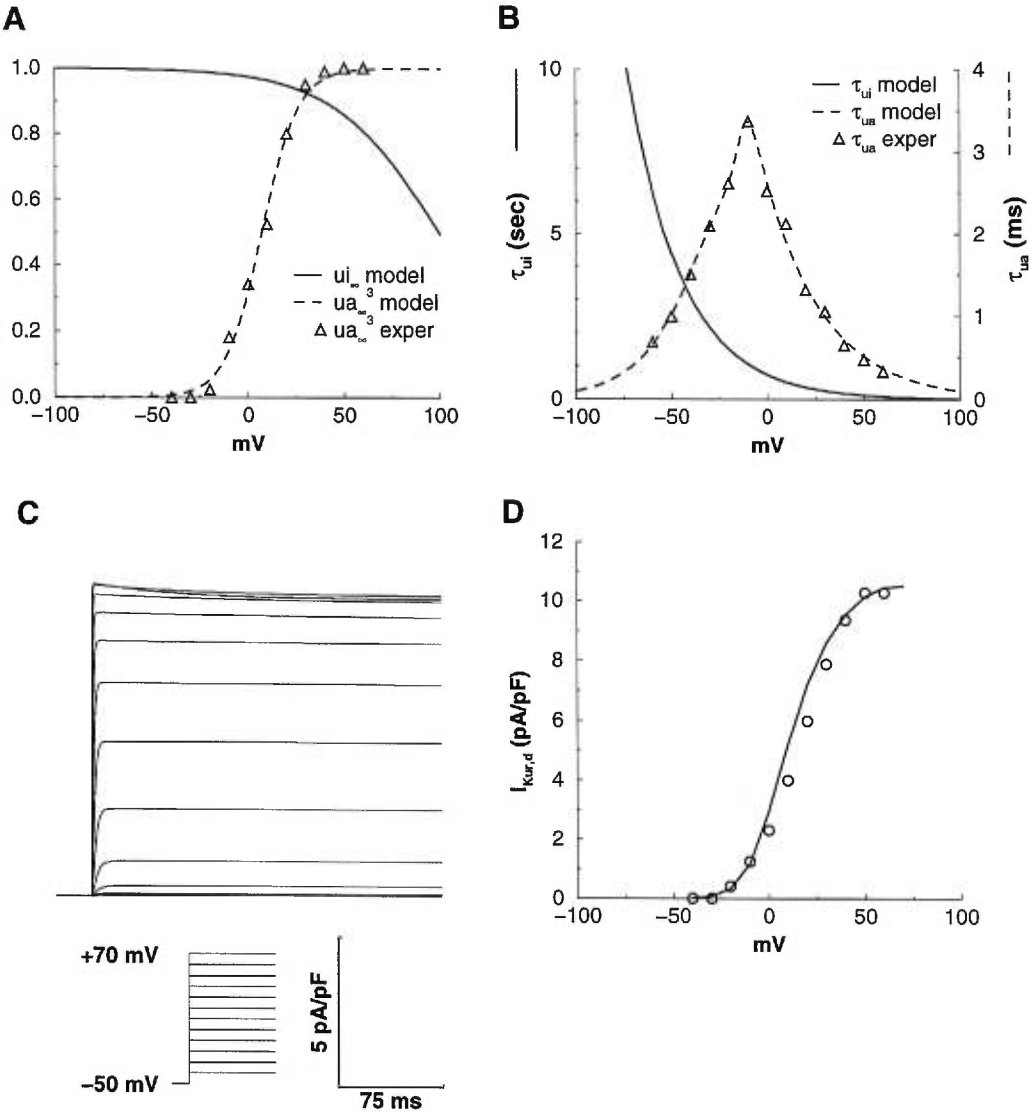

Figure 2.3: Ultrarapid delayed rectifier K^+ current, $I_{Kur,d}$. (A) Activation (dashed line) and inactivation (solid line) steady state values and corresponding experimental data. (B) Time constant values for activation (dashed line) and inactivation (solid line). Triangles represent experimental values for activation (above -10 mV) and deactivation (below -10 mV) (C) $I_{Kur,d}$ response to voltage steps in the model (pulse protocol in inset). (D) Peak $I - V$ relation for model (line) and in experiments (circles).

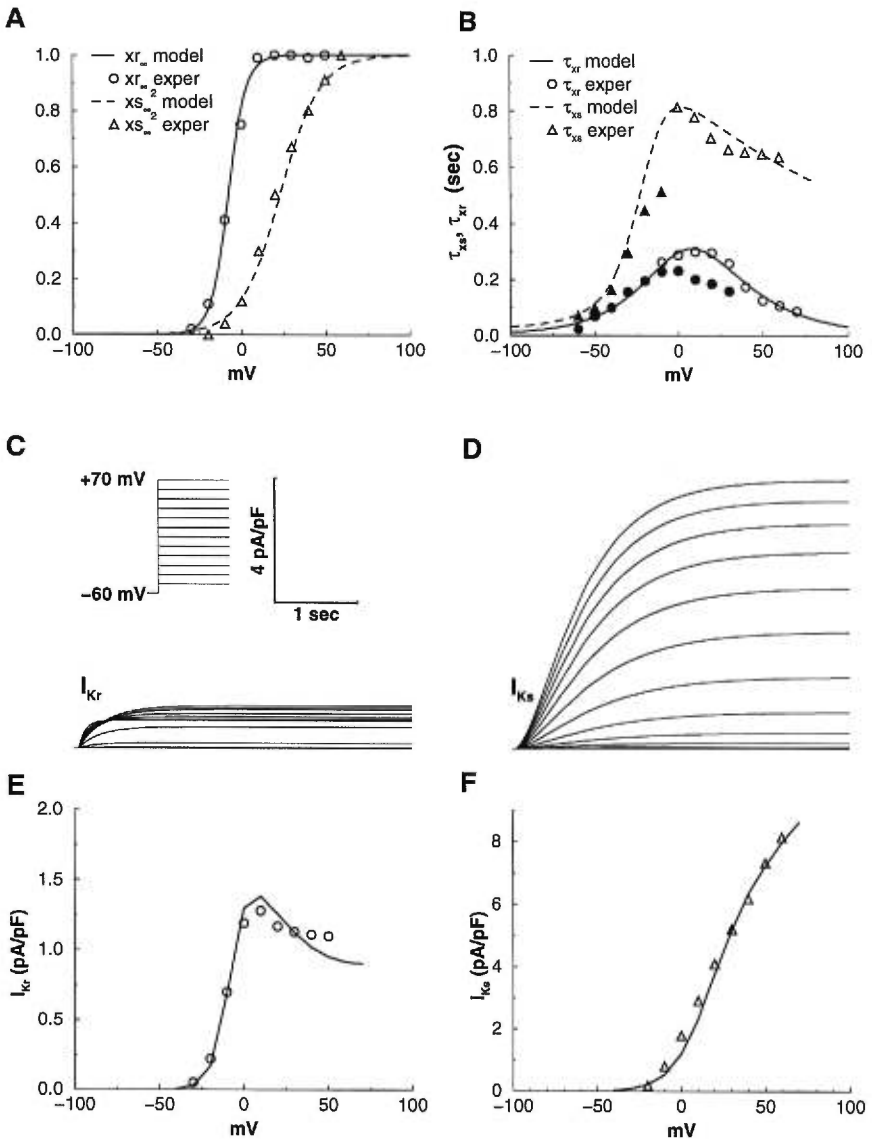

Figure 2.4: Rapid and slow components of the delayed rectifier K^+ current, I_{Kr} and I_{Ks}. (A) Steady state activation for I_{Kr} (solid line) and I_{Ks} (dashed line). Corresponding experimental values are shown with circles and triangles. (B) Time constants for I_{Kr} (solid line) and I_{Ks} (dashed line). Experimental data (symbols) shows time constants for activation and deactivation, at more positive and negative potentials, respectively. Open symbols are data obtained during voltage steps, filled symbols are data from tail currents. (C and D) Responses to voltage steps in the model (pulse protocol in inset). (E and F) Peak $I - V$ relations for model (lines) and in experiments (circles, triangles).

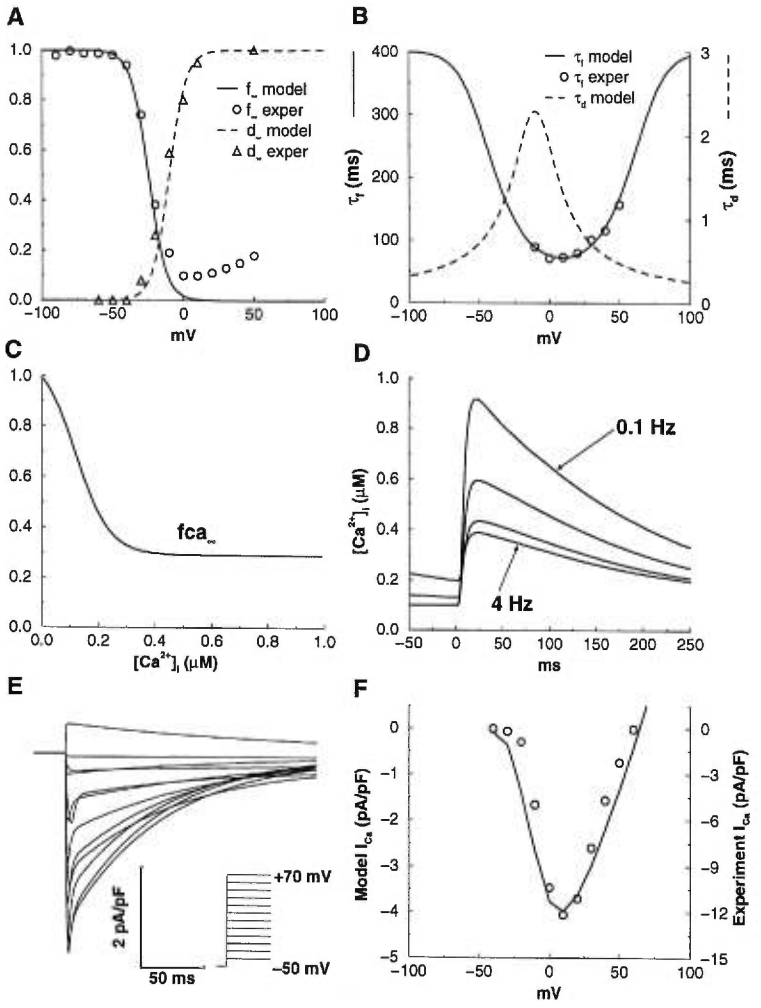

Figure 2.5: Sarcolemmal Ca^{2+} current, I_{Ca}. (A) Voltage-dependent activation (dashed line) and inactivation (solid line) steady state values and corresponding experimental data. (B) Time constant values for activation (dashed line) and inactivation (solid line) and corresponding experimental data. (C) $[Ca^{2+}]_i$-dependent inactivation at steady state. (D) Ca^{2+}-transients generated during activity at 0.1 Hz, 1 Hz, 2 Hz, and 4 Hz. (E) I_{Ca} response to voltage steps (pulse protocol in inset). (F) Peak $I - V$ relation for model (line) and experiment (circles).

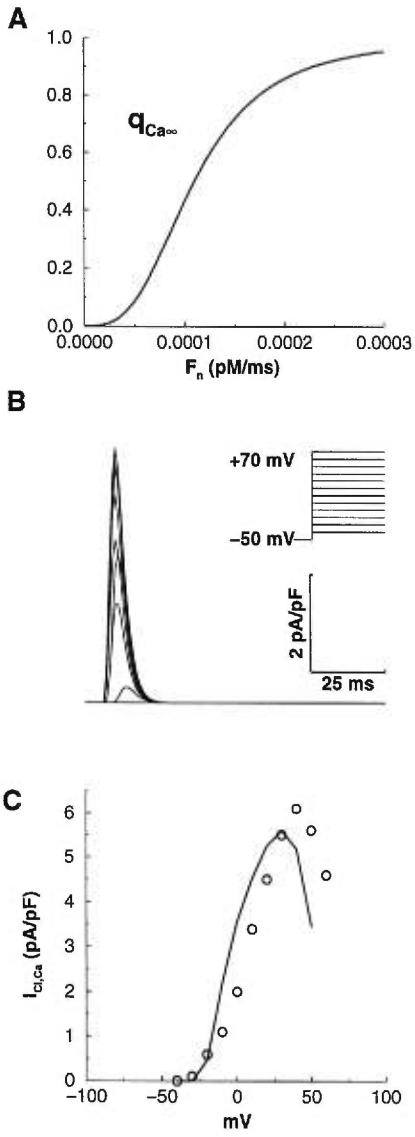

Figure 2.6: Ca^{2+}-activated Cl^- current, $I_{Cl,Ca}$. (A) $I_{Cl,Ca}$ activation at steady state ($q_{Ca\infty}$) depends on a sarcolemmal Ca^{2+} flux signal (F_n). (B) Response to voltage steps (pulse protocol in inset). (C) Peak $I - V$ relation for model (line) and in experiments (circles).

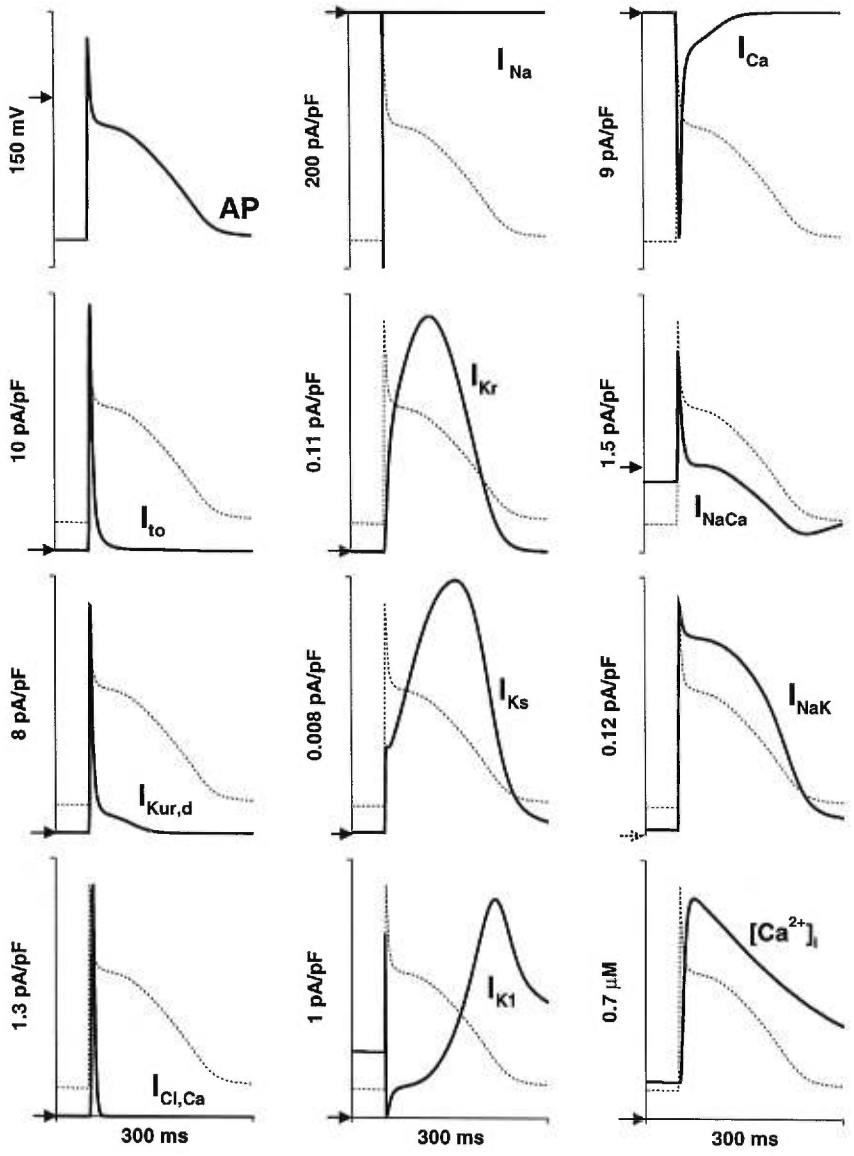

Figure 2.7: Model AP (top left), underlying membrane currents, and $[Ca^{2+}]_i$-transient during AP (lower right). For reference, dashed lines show the time course of the AP to compare with corresponding currents. Solid arrows on the y-axes indicate the zero reference (0 mV for the AP, 0 pA/pF for currents, 0 μM for $[Ca^{2+}]_i$). The dashed arrow on the y-axis for I_{NaK} indicates the baseline value of 0.13 pA/pF. Recordings are taken during the tenth pulse from rest during activity at 1 Hz.

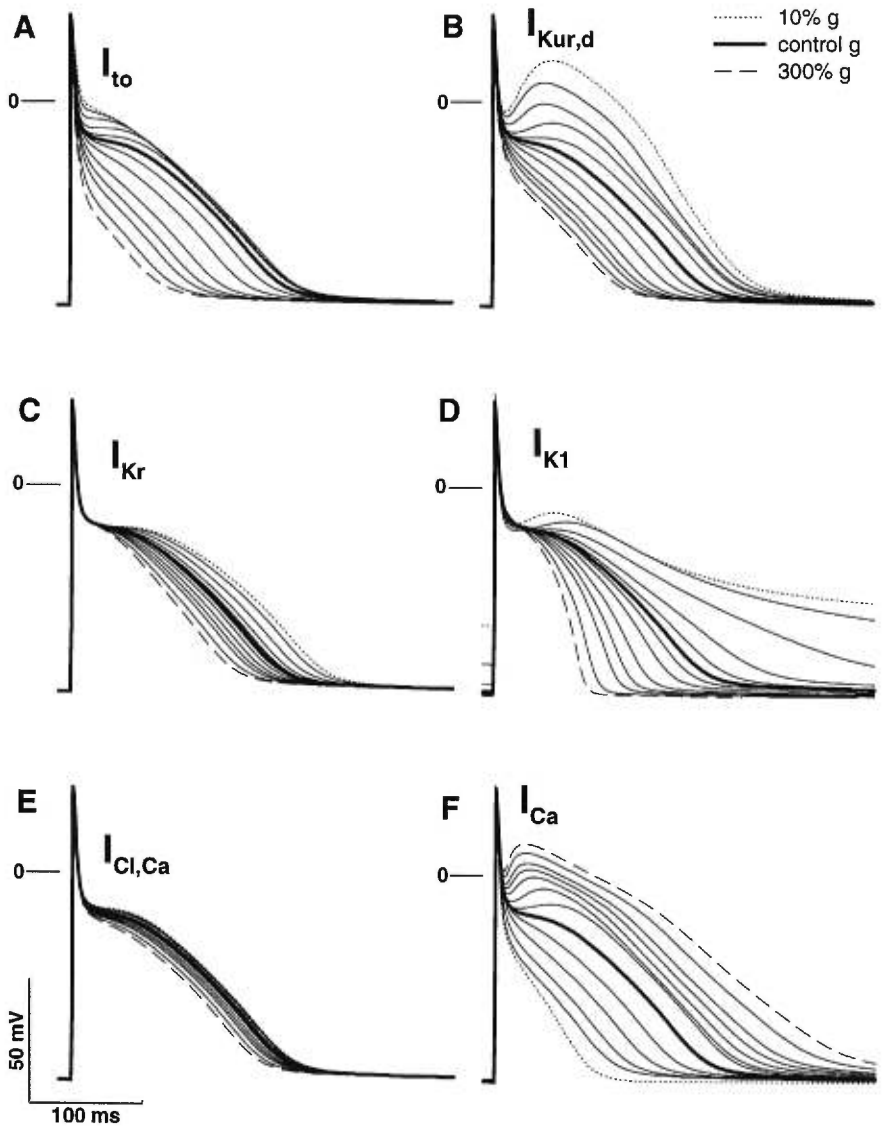

Figure 2.8: Effect of varying (A) I_{to}, (B) $I_{Kur,d}$, (C) I_{Kr}, (D) I_{K1}, (E) $I_{Cl,Ca}$, and (F) I_{Ca} conductance on model AP morphology. Lines correspond to conductances adjusted to 10% (dotted lines), 25, 50, 75, 90, 100 (bold lines), 110, 125, 150, 200, 250, and 300% (dashed lines) of control.

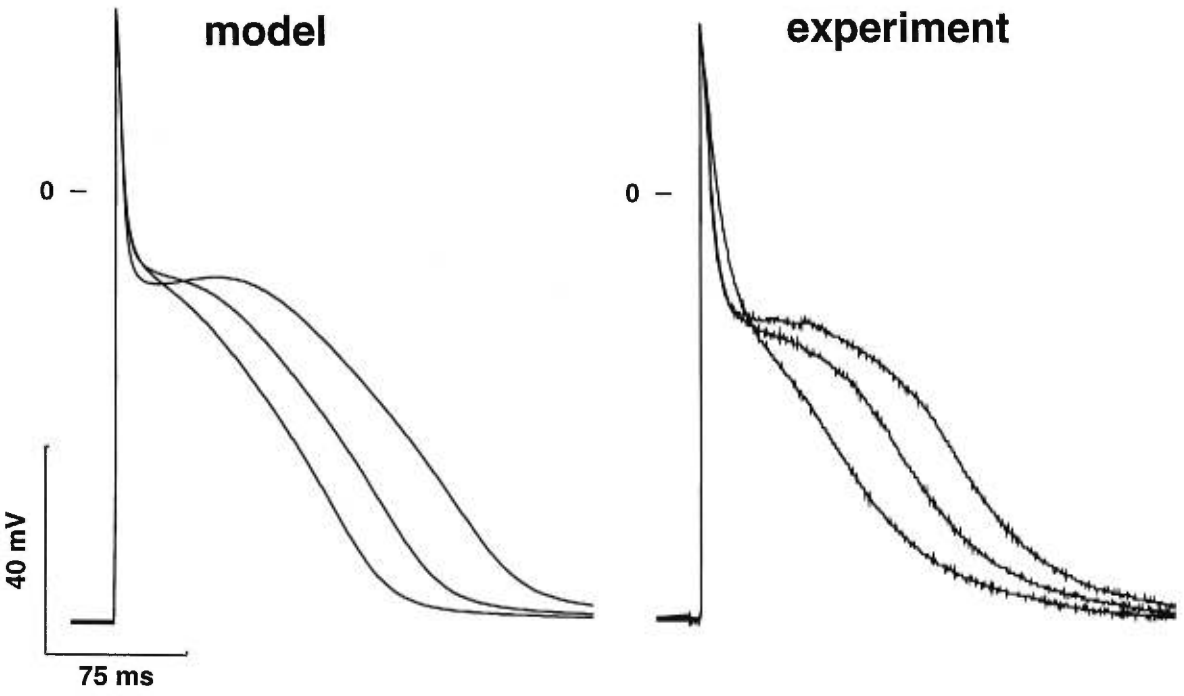

Figure 2.9: Rate-adaptation. Model APs (left) at frequencies of 0.1 Hz (longest APD), 1, and 2 Hz. Representative APs obtained from an isolated canine atrial myocyte (right) at pacing frequencies of 0.1 Hz (longest APD), 1, and 2 Hz.

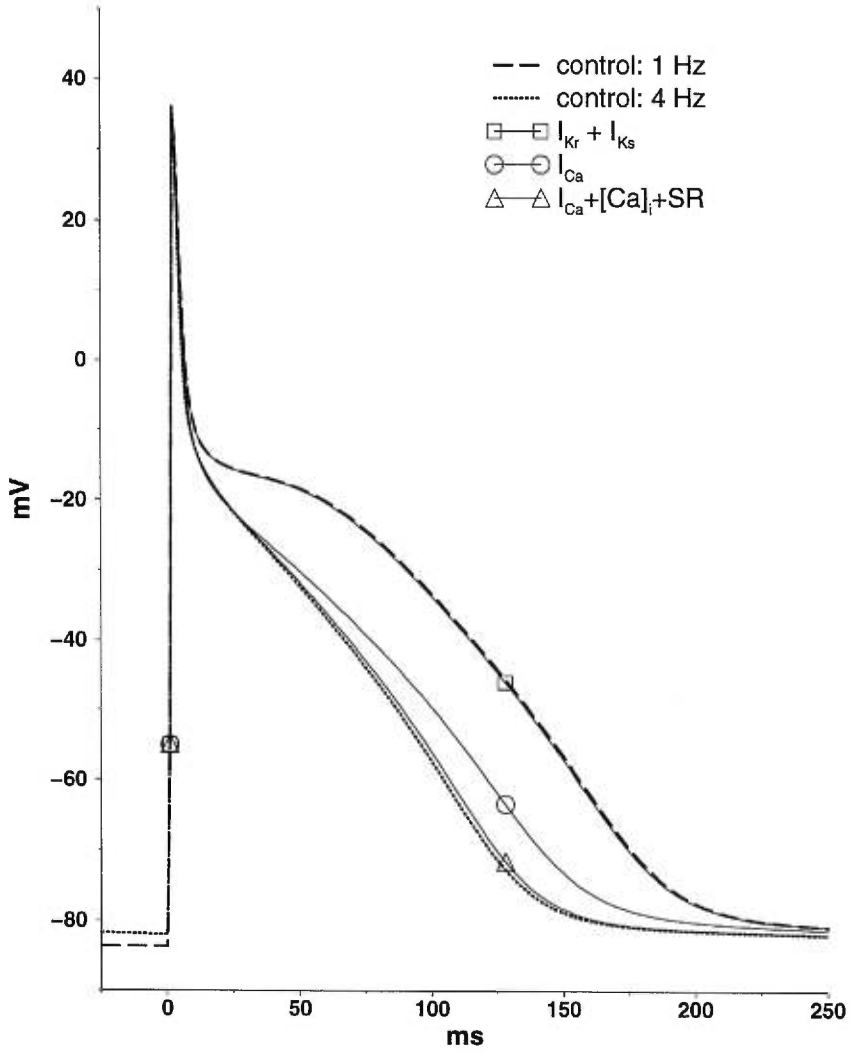

Figure 2.10: Role of I_K, I_{Ca}, and $[Ca^{2+}]_i$ in adaptation of AP in the model to changes in rate. Model AP at 1 Hz (thick dashed line) and at 4 Hz (thick dotted) are shown. Thin traces with symbols indicate the contribution of specified variables to rate-adaptation of the AP (see text for details). Square symbol, activation of I_{Kr} and I_{Ks} combined. Circle, voltage-dependent inactivation of I_{Ca} alone. Triangle, voltage-dependent I_{Ca} inactivation and intracellular Ca^{2+} concentrations.

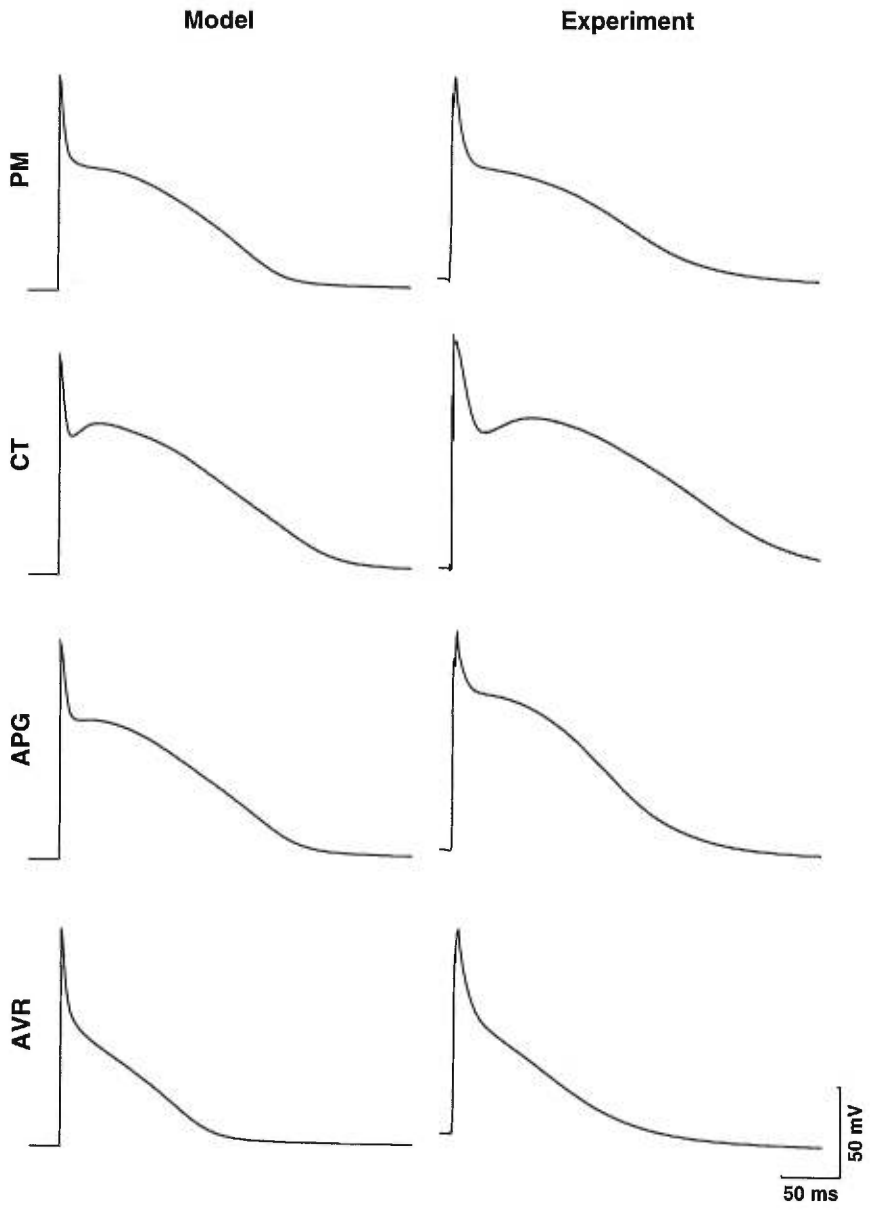

Figure 2.11: Relationship between experimentally observed regional AP heterogeneity and model predictions based on measured variations in ionic currents. Model APs (left column) are compared to digitally averaged APs from Feng *et al.* [17] (right column) in four regions of the canine right atria. PM = pectinate muscle, CT = crista terminalis, APG = appendage, AVR = AV ring region.

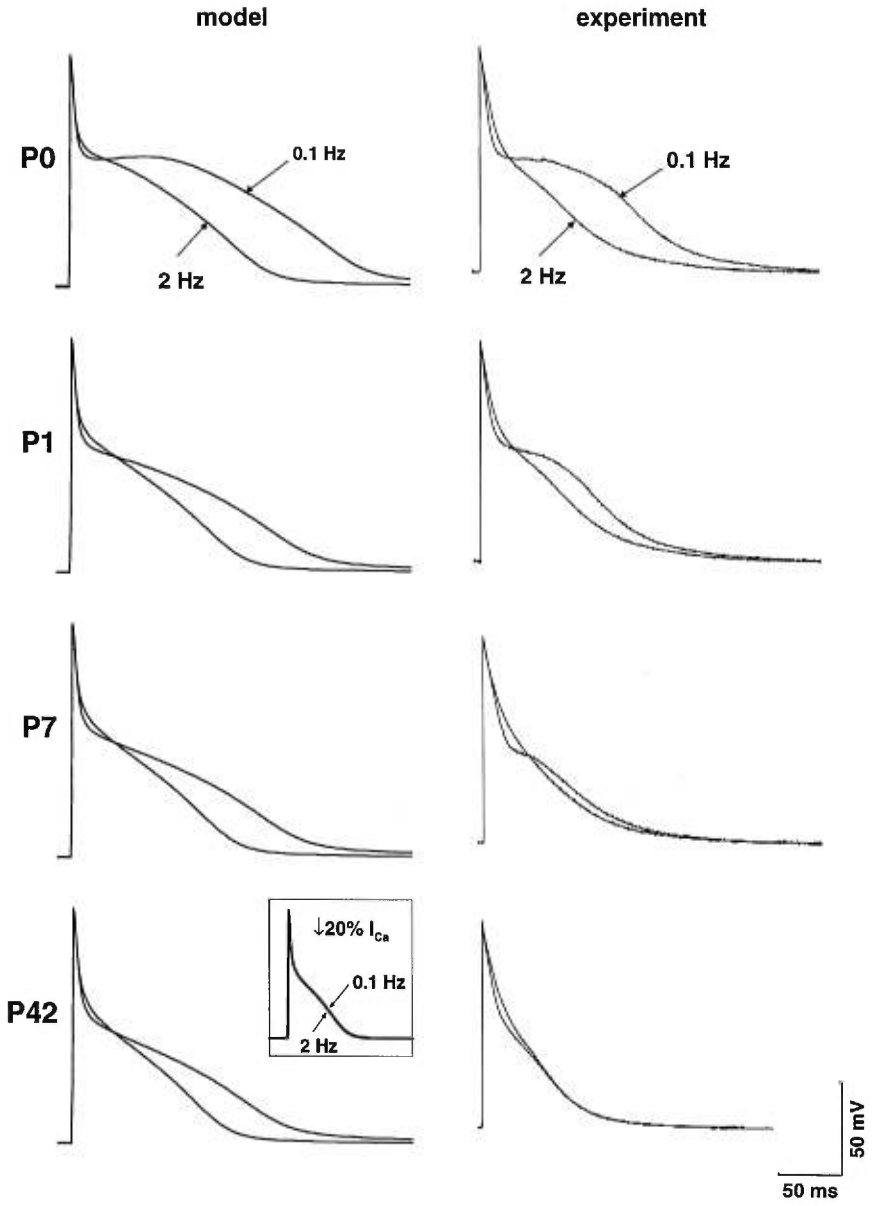

Figure 2.12: Model APs (left column) and AP recordings from a representative canine myocyte from Yue et al [73] (right column) at frequencies of 0.1 and 2 Hz. Myocytes are from dogs subjected to 0, 1, 7, and 42 days of rapid atrial pacing (P0, P1, P7, and P42, respectively). Adaptation to rate is abolished with reduced I_{Ca}. Inset shows model P42 simulations of APs paced at 0.1 and 2 Hz with an additional 20% reduction in I_{Ca}.

Chapter 3

Discussion

3.1 Limitations of the Model

3.1.1 Scaled Current Densities

The canine atrial AP model is based, whenever possible, on experimental data obtained from isolated canine atrial myocytes. The maximal current conductances for I_{to}, $I_{Kur,d}$, I_{Kr}, I_{Ks}, and $I_{Cl,Ca}$ are adjusted to obtain current-voltage relationships that agree well with reported data. Experimental investigations of ionic currents often select for cells with large current amplitudes. This common practice may introduce an experimental bias that, when integrated into a complete mathematical AP model, may require additional scaling in order to simulate observed AP properties. In the present canine atrial AP model, it was sufficient to scale down only the calcium current, I_{Ca}, in order to obtain appropriate AP properties. This raises the question of how one decides which currents need scaling, and by how much. It is possible that similar AP properties may be generated by utilizing different combinations of scaled currents and scaling factors. In this dog AP model, it is possible that by scaling up the amplitudes of the delayed

rectifier currents, I_{Ca} may have required a smaller degree of down-scaling; in such a scenario, it would be possible that results from the model simulations of rate-adaptation and electrical remodeling might have been different than those presented. This limitation is unavoidable in mathematical AP models that are based on experimental data, given the inherent limitations of available laboratory technologies. When drawing inferences from mathematical models, we must keep in mind that despite large variations in AP properties often observed even within small regions from the same preparation, individual model parameters are intended to represent central tendencies of experimentally measured values. A strength of the modeling approach is that it raises questions that can be taken back to the laboratory for further experimental verification.

3.1.2 Canine-Specific Data

The formulation of ionic currents is based on experimental data obtained from canine atrial myocytes whenever canine-specific data was available. However, some transmembrane currents have not been well characterized specifically in canine atrial myocytes. In particular, model descriptions for the Na^+/Ca^{2+} exchanger (I_{NaCa}), the Na^+-K^+ pump (I_{NaK}), and the calcium pump ($I_{p,Ca}$) follow the formulations used by Luo and Rudy [41] for the guinea pig ventricular myocyte. It is possible that the present descriptions of these currents are not fully representative of their properties in the *in situ* canine atrial myocyte. The significant role of intracellular calcium in rate-adaptation implicates I_{NaCa}, which may also play a role in AF-induced electrical remodeling. Repercussions, if any,

for the lack of canine-specific data characterizing I_{NaCa}, I_{NaK}, or $I_{p,Ca}$ in the model are undetermined. Inaccurate representations of current amplitudes potentially contributes to the required scaling of I_{Ca} outlined above.

3.1.3 Delayed Rectifier Currents

Similarities between human and canine delayed rectifier current components in atrial myocytes [67, 71] make the dog a useful species in which to study the role of these currents in arrhythmia mechanisms. The lack of a response of model APs to changes in I_{Ks}, and the absence of a contribution of the delayed rectifiers in mediating adaptation to changes in rate was unexpected, as experimental evidence suggests otherwise in canine ventricular tissue [37]. This possibly dictates two conclusions. First, based on results presented here and in the CRN human AP model [11], human and canine atrial myocytes may differ in their mechanisms of mediating adaptation of AP properties to changes in rate. The CRN model suggests that the delayed rectifiers play an important role in APD shortening at faster rates. However, in canine atrial myocytes, deactivation kinetics are less than 100 ms near resting potentials (figure 2.4B), allowing I_K to recover sufficiently. This restricts the diastolic accumulation of I_K and limits the direct role of I_K in rate-adaptation. In the model, I_{Ks} activation is too slow around plateau potentials to affect significantly AP morphology. Second, the present descriptions for the delayed rectifier current components in canine atria have limitations that may require further investigation. A reevaluation of the delayed rectifiers would be essential to examine drug

effects such as the reverse rate dependence of I_{Kr} blockers on APD [24, 30]. Formulations of I_{Kr} and I_{Ks} are compromises between development of a simple model representation and experimental evidence suggesting more complex gating behavior: (i) activation of I_{Ks} in canine atrial myocytes may exhibit biphasic kinetics with time constants around 1.6 and 0.3 seconds [independent, unpublished reports by Danshi Li and Lixia Yue], and (ii) inspection of patch-clamp recordings of I_{Kr} suggests possible slow inactivation that is not well characterized [17, 71].

3.1.4 Chloride Current

The gating mechanisms and physiological role of the calcium-activated chloride current, $I_{Cl,Ca}$, in canine atria are not well characterized. The absence of selective pharmacological blockers for $I_{Cl,Ca}$ has hindered an electrophysiological approach to explaining its properties. Two commonly used Cl^- channel blockers, DIDS and SITS (disulfonic stilbenes), have been shown to significantly affect Kv4.2 and Kv4.3 K^+ channels [68] which are believed to contribute to I_{to}.

Intracellular calcium, and particularly calcium release from the sarcoplasmic reticulum (SR), plays a central role in mediating $I_{Cl,Ca}$ [10, 74]. Yet, despite the close coupling of sarcolemmal calcium channels and SR release channels, significant reductions in I_{Ca} density in a tachycardia-induced AF model in dogs are not accompanied by corresponding alterations in $I_{Cl,Ca}$ [73]. To my knowledge, there is no publication characterizing

in detail the calcium concentration-dependence of $I_{Cl,Ca}$ activation. As a result, the formulation of $I_{Cl,Ca}$ activation in this model is empirically based on calcium flux within a localized region approximating the closely coupled sarcolemmal calcium channels and SR release channels. Using this approach to formulate $I_{Cl,Ca}$, the peak current-voltage (I-V) relationship in the model (figure 6) shows reasonable agreement with experimental observations [73]. It should be noted, however, that the voltage-dependence suggested in I-V relationships of $I_{Cl,Ca}$ may merely be a reflection of the voltage-dependent properties of I_{Ca} that mediate the calcium-transient and possibly $I_{Cl,Ca}$, and not a true indication of the voltage-dependence of $I_{Cl,Ca}$ *per se*, if such a relationship indeed exists.

3.1.5 Intracellular Calcium Handling

The limitations in describing $I_{Cl,Ca}$ activation in the model are perhaps more deeply rooted in our restricted understanding of intracellular calcium handling mechanisms. Intracellular calcium plays a prominent role in numerous contractile and metabolic processes, many of which exceed the scope of this mathematical AP model. However, some principles governing the excitation-specific properties of calcium handling are still not fully understood in canine atria, such as the nature of coupling between SR calcium release channels and the sarcolemmal calcium channel, and the gating properties of uptake and release of calcium from the SR. The model uses an intracellular SR component for calcium sequestration. The SR appears to be structurally and functionally divided into two components [32, 54], and in the model, is separated into network (NSR) and junctional

(JSR) compartments to mediate uptake and release of calcium. Calcium influx through the sarcolemmal calcium channels (I_{Ca}) initiates a cascade of events that includes a rapid release of calcium from the SR, recruitment of $I_{Cl,Ca}$, a calcium-dependent component of I_{Ca} inactivation, reuptake of calcium into the SR, and equilibration of calcium concentration within the uptake and release compartments of the SR. This calcium handling scheme approximates the principal components of calcium-induced calcium release. It has been suggested that the SR release compartment (JSR in the model) is further compartmentalized into central (or corbular) and peripheral components that have distinct release kinetics and impart a biphasic morphology to the intracellular calcium-transient ($[Ca]_i$) [28].

Jafri, Rice and Winslow (JRW) recently described the calcium-dependent inactivation of I_{Ca} and calcium handling in a mathematical model of a mammalian ventricular myocyte [31]. The JRW model uses the Luo-Rudy (phase II) model [41] to describe transmembrane ionic currents as a basis for their revised model of intracellular calcium-handing. The JRW model implements a multi-state model to describe I_{Ca} activity in the presence and absence of local Ca^{2+}, and uses a 4-state model to describe Ca^{2+}-release from the SR. Their implementation of I_{Ca} involves ten nonconducting states (five each in the presence and absence of Ca^{2+}), and two conducting states, where channel open probability is low in the presence of calcium (conductance is 500 times slower than in absence of Ca^{2+}). An important difference between the JRW model and calcium handling in the present model, and in the CRN model, is the implementation of calcium-dependent

inactivation of I_{Ca}. In the JRW model this inactivation is ligand-gated and mediated by local rather than bulk calcium. The present model uses bulk intracellular calcium to determine the amount of calcium-dependent inactivation of I_{Ca}.

3.1.6 Calcium Currents

This model implements I_{Ca} based on data for L-type calcium channels reported experimentally [73]. T-type calcium channels are also present in atrial myocytes with a reported occurrence of 40% in canine atria [34]. The T-type Ca^{2+} current activates and inactivates rapidly with strong voltage-dependence [62]. In canine atrial myocytes, the maximal T-type I_{Ca} is elicited by depolarizations around -20 mV with a threshold depolarization of about -50 mV; for L-type I_{Ca}, the maximal current is elicited by depolarizations around +10 mV with a threshold depolarization of about -40 mV [34, 73]. The current density amplitude of T-type I_{Ca} is small (only about 6% that of L-type I_{Ca}) [34, 73]. Thus, due to its low occurrence and small amplitude compared to L-type channels, T-type calcium current was not included in this model.

3.1.7 Conservation Effects

Long-term pacing simulations in the model (longer than 4 hours) reveal non-decaying instabilities in the intracellular ion concentrations. During the first fifteen minutes of pacing at 1 Hz from rest, the peak intracellular calcium-transient undergoes an initial rapid decline that decays within the first ten seconds (peak $[Ca^{2+}]_i$ is 0.937 μM at the

first AP and declines to 0.595 μM on the eleventh AP), with little change (about 0.05 μM) over the subsequent fifteen minutes. All model AP recordings shown in chapter 2 are thus taken ten seconds from rest. Following the initial transient, however, slower ionic changes persist. Intracellular potassium concentration, $[K^+]_i$, begins to slowly increase. This increase persists almost linearly for at least the next four hours, with an average slope of about 1.24 mM/hr (<0.9% the initial $[K^+]_i$ per hour) and shows no indication of stabilizing. This phenomenon of long-term ionic instability is common to ionic models that monitor ionic balance, as proven by Varghese and Sell [61] and noted in the CRN human atrial AP model [11]. The AP model of Nygren *et al* attempted to rectify this problem by implementing an "electroneutral Na^+ current" [52] as a corrective factor. This ionic instability permits unbounded changes in intracellular ionic concentrations that may lead to numerical instabilities, particularly in the calculation of I_{NaCa}, for which Varghese and Sell give a modified formulation [61] based on the DiFrancesco-Noble model [14].

The problem of long-term ionic instability lies in the mathematical formulation of the system of differential equations [27]. The system gives explicit time-derivative formulations for membrane potential, gating variables, and all intracellular ion concentrations. The stable steady state, or fixed point, of this system can be determined by obtaining the homogeneous solution of the system, that is, simultaneously equating all time-derivatives to zero and solving. However, by Faraday's principle, total charge (or ionic concentration in the model) is equal to the product of membrane capacitance and potential difference (charge $= C_m \cdot V_m$). Thus, the homogeneous system is not independent; that is, the

steady state of the system is the solution of $n + 1$ equations with n unknowns, since V_m will be proportional to the total intracellular ionic concentrations. The homogeneous solution, or steady state of the system, is therefore represented by a set of nonisolated fixed points. In the canine atrial AP model, each stimulus current, I_{stim}, represents a perturbation of the system away from a fixed point. Equilibration of the system, via repolarization of the cell, would return the system to a fixed point, but not necessarily the same fixed point as that prior to the stimulus. Over the course of a single AP, this change in equilibrium would be infinitesimal. But over several hours of pacing, or thousands of beats, this numerical artifact is magnified. A simple test to verify this phenomenon in the model would be to obtain and compare steady state values before and after a fixed duration of pacing. The present study did not involve any stimulation protocols that exceeded eleven seconds, and so, did not warrant modification to rectify this limitation. Future studies that wish to consider the long-term dynamics of AP properties in the model would require modifications to account for this conservation principle. Guan *et al* outline possible numerical methods that satisfy this conservation principle [27] in the DiFrancesco Noble model. The modifications involve fixing either $\frac{d}{dt}[Na^+]_i$ or $\frac{d}{dt}[K^+]_i$ (or both) equal to zero and treating the associated variable, either $[Na^+]_i$ or $[K^+]_i$ (or both), as a parameter.

In addition, the stimulus current, I_{stim}, which simulates an experimental injection of charge, is fixed at -2900 pA, but its associated charge is not assigned to any specific

intracellular ionic pool. By designating K^+ as the charge carrier for I_{stim} in the model** there were no detectable changes in AP responses during any of the model simulations presented in chapter 2. Long-term effects on numerical stability in the model by an unassigned injected current (I_{stim}) are undetermined.

3.2 Potential Model Improvements

In spite of attempts to use only results specific to canine atrial myocytes in the formulation of the model, such data was sometimes unavailable. Certain experimental procedures would reveal important aspects of the canine atrial action potential and atrial fibrillation, and provide a stronger basis for this model. The following section outlines some possible experimental investigations that would settle uncertainties and help to improve the model.

An improved description of the model delayed rectifiers is important. Confirmation and characterization of I_{Kr} and I_{Ks} inactivation, if it exists, may be important for examining reverse rate dependent effects in the model. This might be achieved with the use of a long pulse protocol. Also, the development of channel-specific blockers for I_{Ks} would help identify the specific role of this current in AP morphology and adaptation to changes in rate.

**Assign K^+ as the charge carrier for I_{stim} by including I_{stim} in the calculation of $\frac{d}{dt}[K^+]_i$ (equation A.5 in appendix A).

Some aspects of intracellular calcium-handling are not clear in canine atria. In skeletal muscle cells, a physical protein-protein association between sarcolemmal calcium channels and SR release channels provides a molecular substrate that explains their coupling [44, 57]. No such physical coupling appears to occur in cardiac myocytes. In rat heart cells, release of calcium from SR stores, but not termination of release, is activated by local I_{Ca} [9]. Characterization of the mechanism of termination of SR release would confirm or refute several empirical models. The present canine atrial AP model utilizes SR release inactivation that is dependent on localized calcium flux and exhibits voltage-dependence following the Friedman *et al* modifications [21] of the Luo-Rudy (phase II) model [41].

Similar control mechanisms for $I_{Cl,Ca}$, I_{rel}, and I_{Ca}, via local intracellular calcium, suggest that an additional colocalization of $I_{Cl,Ca}$ channels with the latter two channels may be plausible. Confocal microscopic and calcium fluorescence techniques may shed some light on this conjecture. This approach has shown that cardiac dysfunction associated with heart failure in hypertensive rats results from defective coupling between I_{rel} and I_{Ca} channels, rather than altered channel properties [9]. A similar situation may play a role in canine heart failure models, or even in similar human pathologies. The model fell short in reproducing the complete loss of rate-adaptation after prolonged rapid pacing (figure 12). In this situation as well, altered coupling may contribute to the development or manifestations of electrical remodeling.

3.3 Future Directions

The canine atrial AP model describes the ionic properties of the space-clamped dog atrial myocyte. This work consolidates existing knowledge, suggests possible directions for future research, and serves as a tool to facilitate and supplement experimental work. For example, incomplete agreement between model APs and AF-induced electrically remodeled APs suggests other factors for experimentalists to examine.

This model will be practical for future propagation studies of arrhythmia mechanisms in computer models of canine atrial tissue. The CRN human atrial AP model has recently been implemented to evaluate ionic targets for potential antiarrhythmic drug treatments of atrial fibrillation [12]. Similar findings in the canine atrial AP model would substantiate the CRN model findings, and further validate the use of canine tissues as models in which to study human atrial pathologies.

A reexamination of the delayed rectifier currents will permit the investigation of mechanisms involved in reverse use dependence. This model can also be used as the basis for a model of intracellular calcium handling and mechanisms involved in excitation-contraction coupling in canine atria.

Appendix A

Model Formulation

Some fractional equations require evaluation of a limit to determine their values at membrane potentials for which their denominator is zero.

$$\frac{dV}{dt} = \frac{-\left(I_{ion} + I_{stim}\right)}{C_m} \tag{A.1}$$

$$\begin{aligned} I_{ion} &= I_{Na} + I_{K1} + I_{to} + I_{Kur} + I_{Kr} + I_{Ks} + I_{CaL} + I_{p,Ca} \\ &\quad + I_{NaK} + I_{NaCa} + I_{b,Na} + I_{b,Ca} + I_{NaK} + I_{NaCa} \end{aligned} \tag{A.2}$$

$$\frac{dy}{dt} = \frac{y_\infty - y}{\tau_y} \qquad (where\ y\ is\ any\ gating\ variable) \tag{A.3}$$

$$\frac{d[Na^+]_i}{dt} = \frac{-3 \cdot I_{NaK} - 3 \cdot I_{NaCa} - I_{b,Na} - I_{Na}}{F\ V_i} \tag{A.4}$$

$$\frac{d[K^+]_i}{dt} = \frac{2 \cdot I_{NaK} - I_{K1} - I_{to} - I_{Kur} - I_{Kr} - I_{Ks} - I_{b,K}}{F\ V_i} \tag{A.5}$$

$$\frac{d[Cl^-]_i}{dt} = \frac{I_{Cl,Ca}}{F\ V_i} \tag{A.6}$$

$$\frac{d[Ca^{2+}]_i}{dt} = \frac{B1}{B2} \tag{A.7}$$

$$B1 \equiv \frac{2\ I_{NaCa} - I_{p,Ca} - I_{Ca,L} - I_{b,Ca}}{2\ F\ V_i} + \frac{V_{up}\left(I_{up,leak} - I_{up}\right) + I_{rel}\ V_{rel}}{V_i} \tag{A.8}$$

$$B2 \equiv 1 + \frac{[Trpn]_{max}\ K_{m,Trpn}}{([Ca^{2+}]_i + K_{m,Trpn})^2} + \frac{[Cmdn]_{max}\ K_{m,Cmdn}}{([Ca^{2+}]_i + K_{m,Cmdn})^2} \tag{A.9}$$

$$\frac{d[Ca^{2+}]_{up}}{dt} = I_{up} - I_{up,leak} - I_{tr}\ \frac{V_{rel}}{V_{up}} \tag{A.10}$$

$$\frac{d[Ca^{2+}]_{rel}}{dt} = (I_{tr} - I_{rel}) \left(1 + \frac{[Csqn]_{max}\ K_{m,Csqn}}{([Ca^{2+}]_{rel} + K_{m,Csqn})^2}\right)^{-1} \tag{A.11}$$

Equilibrium potential

$$E_x = \frac{RT}{zF} log \frac{[x]_o}{[x]_i}, \qquad for\ x = Na^+, K^+, Ca^{2+}, Cl^- \tag{A.12}$$

Fast Na^+ current

$$I_{Na} = g_{Na} \cdot m^3 \cdot h \cdot j\,(V - E_{Na}) \tag{A.13}$$

$$\alpha_m = 0.32\ \frac{V + 47.13}{1 - \exp[-0.1(V + 47.13)]} \tag{A.14}$$

$$\beta_m = 0.08 \exp\left[\frac{V}{-11}\right] \tag{A.15}$$

$$\alpha_h = \begin{cases} 0.135 \exp\left[\frac{V+80}{-6.8}\right] \\ \\ 0, \quad if\ V \geq -40 \end{cases} \tag{A.16}$$

$$\beta_h = \begin{cases} 3.56 \exp[0.079\ V] + 3.1 \cdot 10^5 \exp[0.35\ V] \\ \\ \left(0.13 \left(1 + \exp\left[\frac{V + 10.66}{-11.1}\right]\right)\right)^{-1}, \quad if\ V \geq -40 \end{cases} \tag{A.17}$$

$$\alpha_j = \begin{cases} (V+37.78)\dfrac{\left(127140\exp[0.2444\,V] \;+\; 3.474\cdot 10^{-5}\exp[-0.04391\,V]\right)}{-1-\exp[0.311(V+79.23)]} \\ \\ 0, \quad if\ V \geq -40 \end{cases} \tag{A.18}$$

$$\beta_j = \begin{cases} 0.1212\ \dfrac{\exp[-0.01052\,V]}{1+\exp[-0.1378(V+40.14)]} \\ \\ 0.3\ \dfrac{\exp[-2.535\cdot 10^{-7}\,V]}{1+\exp[-0.1(V+32)]},\ if\ V \geq -40 \end{cases} \tag{A.19}$$

$$\tau_\phi = (\alpha_\phi + \beta_\phi)^{-1} \quad and \quad \phi_\infty = \alpha_\phi \tau_\phi, \qquad for\ \phi = m, n, j \tag{A.20}$$

Time-independent inward rectifier K^+ current

$$I_{K1} = \frac{g_{K1}(V - E_K)}{1+\exp[0.07(V+80)]} \tag{A.21}$$

Transient outward K^+ current

$$I_{to} = g_{to}\cdot o_a^3 \cdot o_i (V - E_K) \tag{A.22}$$

$$\alpha_{oa} = 0.65\left(\exp\left[\frac{V+18}{-8.5}\right] + \exp\left[\frac{V-16}{-59}\right]\right)^{-1} \tag{A.23}$$

$$\beta_{oa} = 1.2\left(2.2 + \exp\left[\frac{V+75}{18}\right]\right)^{-1} \tag{A.24}$$

$$\tau_{oa} = (\alpha_{oa} + \beta_{oa})^{-1} \tag{A.25}$$

$$oa_\infty = \left(1 + \exp\left[\frac{V+0.5}{-10.5}\right]\right)^{-1/3} \tag{A.26}$$

$$\alpha_{oi} = \left(6.2 + \exp\left[\frac{V+105.2}{9.85}\right]\right)^{-1} \tag{A.27}$$

$$\beta_{oi} = \left(7.54 + \exp\left[\frac{V - 8.89}{-12.87}\right]\right)^{-1} \tag{A.28}$$

$$\tau_{o_i} = (\alpha_{oi} + \beta_{oi})^{-1} \tag{A.29}$$

$$oi_{\infty} = \left(1 + \exp\left[\frac{V + 43.377}{6.45}\right]\right)^{-1} \tag{A.30}$$

Ultrarapid delayed rectifier K^+ current

$$I_{Kur,d} = g_{Kur,d} \cdot u_a^3 \cdot u_i \left(V - E_K\right) \tag{A.31}$$

$$g_{Kur,d} = 0.00855 + \frac{0.0779}{1 + \exp\left[\frac{V + 11}{-16}\right]} \tag{A.32}$$

$$\alpha_{ua} = 1.47 \left(\exp\left[\frac{V + 33.2}{-30.63}\right] + \exp\left[\frac{V - 27.6}{-30.65}\right]\right)^{-1} \tag{A.33}$$

$$\beta_{ua} = 0.42 \left(\exp\left[\frac{V + 26.64}{2.49}\right] + \exp\left[\frac{V + 44.41}{20.36}\right]\right)^{-1} \tag{A.34}$$

$$\tau_{ua} = (\alpha_{ua} + \beta_{ua})^{-1} \tag{A.35}$$

$$ua_{\infty} = \left(1 + \exp\left[\frac{V + 2.9}{-9.49}\right]\right)^{-1/3} \tag{A.36}$$

$$\alpha_{ui} = \left(21 + \exp\left[\frac{V - 185}{-28}\right]\right)^{-1} \tag{A.37}$$

$$\beta_{ui} = \exp\left[\frac{V - 158}{16}\right] \tag{A.38}$$

$$\tau_{ui} = (\alpha_{u_i} + \beta_{u_i})^{-1} \tag{A.39}$$

$$ui_{\infty} = \left(1 + \exp\left[\frac{V - 99.45}{27.48}\right]\right)^{-1} \tag{A.40}$$

Rapid delayed outward rectifier K^+ current

$$I_{Kr} = g_{Kr} \cdot x_r \left(0.07 + \frac{0.58}{1 + \exp[(V+15)/22.4]}\right)(V - E_K) \tag{A.41}$$

$$\alpha_{x_r} = 0.04 \frac{V - 248}{1 - \exp\left[\frac{V-248}{-28}\right]} \tag{A.42}$$

$$\beta_{x_r} = 0.028 \frac{V + 163}{\exp\left[\frac{V+163}{21}\right] - 1} \tag{A.43}$$

$$\tau_{x_r} = (\alpha_{x_r} + \beta_{x_r})^{-1} \tag{A.44}$$

$$x_{r\infty} = \left(1 + \exp\left[\frac{V + 7.654}{-5.377}\right]\right)^{-1} \tag{A.45}$$

Slow delayed outward rectifier K^+ current

$$I_{Ks} = g_{Ks} \cdot x_s^2 (V - E_K) \tag{A.46}$$

$$\alpha_{x_s} = 10^{-5} \frac{V + 28.5}{1 - \exp\left[\frac{V+28.5}{-115}\right]} \tag{A.47}$$

$$\beta_{x_s} = 0.00023 \frac{V + 28.5}{\exp\left[\frac{V+28.5}{3.3}\right] - 1} \tag{A.48}$$

$$\tau_{x_s} = (\alpha_{x_s} + \beta_{x_s})^{-1} \tag{A.49}$$

$$x_{s\infty} = \left(1 + \exp\left[\frac{V - 13}{-12}\right]\right)^{-1/2} \tag{A.50}$$

Sarcolemmal Ca^{2+} current

$$I_{Ca} = g_{Ca} \cdot d \cdot f \cdot f_{Ca}(V - 65) \tag{A.51}$$

$$\tau_d = \frac{1 - \exp\left[\frac{V+10}{-6.24}\right]}{0.035(V+10)\left(1+\exp\left[\frac{V+10}{-6.24}\right]\right)} \tag{A.52}$$

$$d_\infty = \left(1+\exp\left[\frac{V+10}{-6}\right]\right)^{-1} \tag{A.53}$$

$$\tau_f = 400\left(1+4.5\exp\left[-0.0007(V-9)^2\right]\right)^{-1} \tag{A.54}$$

$$f_\infty = \left(1+\exp\left[\frac{V+24.6}{6.2}\right]\right)^{-1} \tag{A.55}$$

$$f_{Ca\infty} = 0.29 + 0.8\left(1+\exp\left[\frac{[Ca^{2+}]_i - 0.00012}{0.00006}\right]\right)^{-1} \tag{A.56}$$

Ca^{2+}-activated Cl^- current

$$I_{Cl,Ca} = g_{Cl,Ca}\cdot q_{Ca}\,(V - E_{Cl}) \tag{A.57}$$

$$q_{Ca\infty} = 1 - \left(1+\left(\frac{F_n}{1.1\cdot 10^{-10}}\right)^3\right)^{-1} \tag{A.58}$$

$Na^+ - K^+$ pump current

$$I_{NaK} = I_{NaK(max)}\cdot f_{NaK}\,\frac{1}{1+(K_{m,Na(i)}/[Na^+]_i)^{1.5}}\cdot\frac{[K^+]_o}{[K^+]_o + K_{m,K(o)}} \tag{A.59}$$

$$f_{NaK} = \left(1+0.1245\exp\left[-0.1\,\frac{FV}{RT}\right]+0.0365\cdot\sigma\cdot\exp\left[-\frac{FV}{RT}\right]\right)^{-1} \tag{A.60}$$

$$\sigma = \frac{1}{7}\left(\exp\left[\frac{[Na^+]_o}{67.3}\right]-1\right) \tag{A.61}$$

Na^+/Ca^{2+} exchanger current

$$I_{Na,Ca} = \frac{I_{NaCa(max)}\left([Na^+]_i^3[Ca^{2+}]_o\exp[\gamma\,\frac{FV}{RT}] - [Na^+]_o^3[Ca^{2+}]_i\exp[(\gamma-1)\frac{FV}{RT}]\right)}{(K_{m,Na}^3+[Na^+]_o^3)(K_{m,Ca}+[Ca^{2+}]_o)(1+k_{sat}\exp[(\gamma-1)\frac{FV}{RT}])} \tag{A.62}$$

Background currents

$$I_{b,Ca} = g_{b,Ca}(V - E_{Ca}) \tag{A.63}$$

$$I_{b,Na} = g_{b,Na}(V - E_{Na}) \tag{A.64}$$

Ca^{2+} pump current

$$I_{p,Ca} = I_{p,Ca(max)} \frac{[Ca^{2+}]_i}{0.0005 + [Ca^{2+}]_i} \tag{A.65}$$

Ca^{2+} release current from JSR

$$I_{rel} = k_{rel} \cdot u^2 \cdot v \cdot w \left([Ca^{2+}]_{rel} - [Ca^{2+}]_i\right) \tag{A.66}$$

$$u_\infty = \left(1 + \exp\left[\frac{F_n - 3.4175 \cdot 10^{-13}}{-13.67 \cdot 10^{-16}}\right]\right)^{-1} \tag{A.67}$$

$$\tau_v = 1.91 + 2.09 \left(1 + \exp\left[\frac{F_n - 3.4175 \cdot 10^{-13}}{-13.67 \cdot 10^{-16}}\right]\right)^{-1} \tag{A.68}$$

$$v_\infty = 1 - \left(1 + \exp\left[\frac{F_n - 6.835 \cdot 10^{-14}}{-13.67 \cdot 10^{-16}}\right]\right)^{-1} \tag{A.69}$$

$$\tau_w = 6 \frac{1 - \exp\left[\frac{V - 7.9}{-5}\right]}{\left(1 + 0.3 \exp\left[\frac{V - 7.9}{-5}\right]\right)(V - 7.9)} \tag{A.70}$$

$$w_\infty = 1 - \left(1 + \exp\left[\frac{V - 40}{-17}\right]\right)^{-1} \tag{A.71}$$

$$F_n = 10^{-12} \cdot V_{rel} \cdot I_{rel} - 5 \cdot 10^{-13} \cdot F^{-1} \left(\frac{1}{2} I_{Ca,L} - \frac{1}{5} I_{NaCa}\right) \tag{A.72}$$

Transfer current from NSR to JSR

$$I_{tr} = \frac{[Ca^{2+}]_{up} - [Ca^{2+}]_{rel}}{\tau_{tr}} \tag{A.73}$$

Ca^{2+} uptake current by the NSR

$$I_{up} = \frac{I_{up(max)}}{1 + (K_{up}/[Ca^{2+}]_i)} \tag{A.74}$$

Ca^{2+} leak current by the NSR

$$I_{up,leak} = I_{up(max)} \frac{[Ca^{2+}]_{up}}{[Ca^{2+}]_{up(max)}} \tag{A.75}$$

Ca^{2+} Buffers

$$[Ca^{2+}]_{Cmdn} = [Cmdn]_{max} \frac{[Ca^{2+}]_i}{[Ca^{2+}]_i + K_{m,Cmdn}} \tag{A.76}$$

$$[Ca^{2+}]_{Trpn} = [Trpn]_{max} \frac{[Ca^{2+}]_i}{[Ca^{2+}]_i + K_{m,Trpn}} \tag{A.77}$$

$$[Ca^{2+}]_{Csqn} = [Csqn]_{max} \frac{[Ca^{2+}]_{rel}}{[Ca^{2+}]_{rel} + K_{m,Csqn}} \tag{A.78}$$

Numerical integration

At time step p, the updated value of a time-dependent variable is given by

$$\chi^{(p)} = \chi^{(p-1)} + \triangle t \, \frac{d\chi}{dt} \tag{A.79}$$

for χ = V or any time-dependent ionic concentration, and

$$y^{(p)} = y_\infty + \left(y^{(p-1)} - y_\infty\right) \exp\left[-\frac{\triangle t}{\tau_y}\right] \tag{A.80}$$

for y = any gating variable.

Appendix B

Model Constants

Symbol	Definition	Value
R	Gas constant	8.3143 $J/(K \cdot mol)$
T	Temperature	310 K
F	Faraday constant	96.4867 C/mmol
C_m	Membrane capacitance	100 pF
V_{cell}	Cell volume	20100 μm^3
V_i	Intracellular volume	13668 μm^3
V_{up}	SR uptake compartment (NSR) volume	1109.52 μm^3
V_{rel}	SR release compartment (JSR) volume	96.48 μm^3
$[K^+]_o$	Extracellular potassium concentration	5.4 mM
$[Na^+]_o$	Extracellular sodium concentration	140 mM
$[Ca^{2+}]_o$	Extracellular calcium concentration	1.8 mM
$[Cl^-]_o$	Extracellular chloride concentration	132 mM
g_{Na}	Maximal I_{Na} conductance	7.8 nS/pF
g_{K1}	Maximal I_{K1} conductance	0.15 nS/pF
g_{to}	Maximal I_{to} conductance	0.19824 nS/pF
g_{Kr}	Maximal I_{Kr} conductance	0.06984 nS/pF
g_{Ks}	Maximal I_{Ks} conductance	0.0561 nS/pF
g_{Ca}	Maximal $I_{Ca,L}$ conductance	0.24 nS/pF
$g_{Cl,Ca}$	Maximal $I_{Cl,Ca}$ conductance	0.23 nS/pF
$g_{b,Ca}$	Maximal $I_{b,Ca}$ conductance	0.00113 nS/pF
$g_{b,Na}$	Maximal $I_{b,Na}$ conductance	0.000674 nS/pF
$I_{NaK(max)}$	Maximal I_{NaK} current	0.6 pA/pF
$I_{NaCa(max)}$	Maximal I_{NaCa} current	1600 pA/pF
$I_{p,Ca(max)}$	Maximal $I_{p,Ca}$ current	0.275 pA/pF
$I_{up(max)}$	Maximal I_{up} current	0.005 mM/ms
τ_{fca}	Ca^{2+}-dependent I_{Ca} inactivation time constant	2 ms
τ_{qca}	Ca^{2+}-dependent $I_{Cl,Ca}$ activation time constant	2 ms
τ_{tr}	Ca^{2+} transfer time constant	180 ms
τ_u	I_{rel} activation time constant	8 ms
γ	Voltage-dependence parameter for I_{NaCa}	0.35
$K_{m,Na(i)}$	$[Na^+]_i$ half-saturation constant for I_{NaK}	10 mM
$K_{m,K(o)}$	$[K^+]_o$ half-saturation constant for I_{NaK}	1.5 mM
$K_{m,Na}$	$[Na^+]_o$ half-saturation constant for I_{NaCa}	87.5 mM
$K_{m,Ca}$	$[Ca^{2+}]_o$ half-saturation constant for I_{NaCa}	1.38
k_{sat}	Saturation factor for I_{NaCa}	0.1
k_{rel}	Maximal release rate for I_{rel}	30 ms^{-1}
K_{up}	$[Ca^{2+}]_i$ half-saturation constant for I_{up}	0.00092 mM
$[Ca^{2+}]_{up(max)}$	Maximal Ca^{2+} concentration in NSR	15 mM
$[Cmdn]_{max}$	Total calmodulin concentration in myoplasm	0.05 mM
$[Trpn]_{max}$	Total troponin concentration in myoplasm	0.07 mM
$[Csqn]_{max}$	Total calsequestrin concentration in JSR	10 mM
$K_{m,Cmdn}$	$[Ca^{2+}]_i$ half-saturation constant for calmodulin	0.00238 mM
$K_{m,Trpn}$	$[Ca^{2+}]_i$ half-saturation constant for troponin	0.0005 mM
$K_{m,Csqn}$	$[Ca^{2+}]_{rel}$ half-saturation constant for I_{up}	0.8 mM

Appendix C

Initial Conditions

Symbol	Resting Value	Definition
V	-83.53 mV	Resting membrane potential
m	0.001972	I_{Na} activation variable
h	0.9791	I_{Na} fast inactivation variable
j	0.9869	I_{Na} slow inactivation variable
d	$4.758{\cdot}10^{-6}$	I_{Ca} activation variable
f	0.9999	I_{Ca} voltage-dependent inactivation variable
x_r	$7.435{\cdot}10^{-7}$	I_{Kr} activation variable
x_s	0.01791	I_{Ks} activation variable
$[Na^+]_i$	11.77 mM	Intracellular Na^+ concentration
$[Ca^{2+}]_i$	0.1026 μM	Intracellular Ca^{2+} concentration
$[K^+]_i$	138.4 mM	Intracellular K^+ concentration
$[Cl^-]_i$	29.26 mM	Intracellular Cl^- concentration
$[Ca^{2+}]_{up}$	1.506 mM	Ca^{2+} concentration in uptake compartment
$[Ca^{2+}]_{rel}$	1.506 mM	Ca^{2+} concentration in release compartment
o_a	0.07164	I_{to} activation variable
o_i	0.9980	I_{to} inactivation variable
q_{Ca}	0.0	$I_{Cl,Ca}$ Ca^+ flux-dependent activation variable
u_a	0.05869	$I_{Kur,d}$ activation variable
u_i	0.9987	$I_{Kur,d}$ inactivation variable
f_{Ca}	0.7475	I_{Ca} Ca^+-dependent inactivation variable
$[Ca^{2+}]_{Cmdn}$	0.002067 mM	Ca^+-bound calmodulin concentration
$[Ca^{2+}]_{Trpn}$	0.01192 mM	Ca^+-bound troponin concentration
$[Ca^{2+}]_{Csqn}$	6.530 mM	Ca^+-bound calsequestrin concentration
u	0.0	I_{rel} activation variable
v	1.0	I_{rel} Ca^+ flux-dependent inactivation variable
w	0.9993	I_{rel} voltage-dependent inactivation variable

Bibliography

[1] **Abildskov, JA** (1996) *Induced termination of fibrillation.* J Cardiovasc Electrophysiol 7:71-81.

[2] **Allesie, MA, WJEP Lammers, FIM Bonke, and SJ Hollen** (1985) *Experimental evaluation of Moe's multiple wavelet hypothesis of atrial fibrillation.* In: DP Zipes, J Jalife, eds. Cardiac Electrophysiology and Arrhythmias. New York: Grune & Stratton, 265-275.

[3] **Attuel, P, R Childers, B Cauchemez, J Poveda, J Mugica, and P Coumel** (1982) *Failure in the rate adaptation of the atrial refractory period: its relationship to vulnerability.* Intl J Cardiol 2:179-197.

[4] **Beeler, GW, and H Reuter** (1977) *Reconstruction of the action potential of ventricular myocardial fibres.* J Physiol (Lond) 268:177-210.

[5] **Boutjdir, M, JY LeHeuzey, T Laverngne, S Chauvaud, L Guize, A Carpentier, and P Peronneau** (1986) *Inhomogeneity of cellular refractoriness in human atrium: factor of arrhythmia?* PACE 9:1095-1100.

[6] **Boyden, PA, and BF Hoffman** (1981) *The effects on atrial electrophysiology and structure of surgically induced right atrial enlargement in dogs.* Circ Res 49(6):1319-1331.

[7] **Boyden, PA, LP Tilley, TD Pham, S-K Liu, JJ Fenoglio Jr., and AL Wit** (1982) *Effects of left atrial enlargement on atrial transmembrane potentials and structure in dogs with mitral valve fibrosis.* Am J Cardiol 49(8):1896-1908.

[8] **Bristow, DG, and JW Clark** (1982) *A mathematical model of primary pacemaking cell in SA node of the heart.* Am J Physiol 243:H207-H218.

[9] **Cannel, MB, H Cheng, and WJ Lederer** (1995) *The control of calcium release in heart muscle.* Science 268:1045-1049.

[10] **Collier, ML, PC Levesque, JL Kenyon, and JR Hume** (1996) *Unitary Cl^- channels activated by cytoplasmic Ca^{2+} in canine ventricular myocytes.* Circ. Res. 78:936-944.

[11] **Courtemanche, M, RJ Ramirez, and S Nattel** (1998) *Ionic mechanisms underlying human atrial action potential properties: insights from a mathematical model.* Am J Physiol 275(Heart Circ Physiol 44): H301-H321.

[12] **Courtemanche, M, RJ Ramirez, and S Nattel** (1999) *Ionic targets for drug therapy and AF-induced electrical remodeling: insights from a mathematical model.* Cardiovasc Res (in press)

[13] **Demir, SS, JW Clark, CR Murphey, and WR Giles** (1994) *A mathematical model of a rabbit sinoatrial node cell.* Am J Physiol 266(Cell Physiol 35):C832-C852.

[14] **DiFrancesco, D, and D Noble** (1985) *A model of cardiac electrical activity incorporating ionic pumps and concentration changes* Philos Trans R Soc Lond Biol 307:353-398.

[15] **Ebihara, L, and EA Johnson** (1980) *Fast sodium current in cardiac muscle: a quantitative description.* Biophys J 32:779-790.

[16] **Fareh, S, C Villemaire, and S Nattel** (1998) *Importance of refractoriness heterogeneity in the enhanced vulnerability to atrial fibrillation induction caused by tachycardia-induced atrial electrical remodeling.* Circulation 98(20):2202-2209.

[17] **Feng, J, L Yue, Z Wang, and S Nattel** (1998) *Ionic mechanisms of regional action potential heterogeneity in the canine right atrium.* Circ Res 83:541-551.

[18] **Feng, J, D Xu, Z Wang, and S Nattel** (1998) *Ultrarapid delayed rectifier current inactivation in human atrial myocytes: properties and consequences.* Am J Physiol 275(Heart Circ Physiol 44):H1717-H1725.

[19] **Fermini, B, Z Wang, D Duan, and S Nattel** (1992) *Differences in rate dependence of transient outward current in rabbit and human atrium.* Am J Physiol 263(Heart Circ Physiol 32):H1747-H1754.

[20] **Firek, L, and WR Giles** (1995) *Outward currents underlying repolarization in human atrial myocytes.* Cardiovasc Res 30:31-38.

[21] **Friedman, N** (1996) *Étude d'un nouveau modèle du myocyte cardiaque incorporant une régulation du calcium intracellulaire* (Master's thesis). Montreal: École Polytechnique de Montréal, Université de Montréal.

[22] **Garrey, WE** (1914) *The nature of fibrillatory contraction of the heart – its relation to tissue mass and form.* Am J Physiol 33:397-414.

[23] **Gaspo, R, RF Bosch, M Talajic, and S Nattel** (1997) *Functional mechanisms underlying tachycardia-induced sustained atrial fibrillation in a chronic dog model.* Circulation 96:4027-4035.

[24] **Gintant, GA** (1996) *Two components of delayed rectifier current in canine atrium and ventricle: does I_{Ks} play a role in the reverse rate dependence of class III agents?* Circ Res 78:26-37.

[25] **Goette, A, C Honeycutt, and JJ Langberg** (1996) *Electrical remodeling in atrial fibrillation: time course and mechanisms.* Circulation 94:2968-2974.

[26] **Gómez, AM, HH Valdivia, H Cheng, MR Lederer, LF Santana, MB Cannell, SA McCune, RA Altschuld, and WJ Lederer** (1997) *Defective excitation-contraction coupling in experimental cardiac hypertrophyand heart failure.* Science 276:800-806.

[27] **Guan, S, Q Lu, and K Huang** (1997) *A discussion about the DiFrancesco-Noble model.* J Theor Biol 189:27-32.

[28] **Hatem, SN, A Bernardeau, C Rucker-Martin, I Marty, P de Chamisso, M Villaz, and J-J Mercadier** (1997) *Different compartments of sarcoplasmic reticulum participate in the excitation-contraction coupling process in human atrial myocytes.* Circ Res 80:345-353.

[29] **Hodgkin, AL, and AF Huxley** (1952) *A quantitative description of membrane current and its application to conduction and excitation in nerve.* J Physiol (Lond) 117:500-544.

[30] **Hondeghem, LM** (1992) *Development of of class III antiarrhythmic agents.* J Cardiovasc Pharmacol 20(Suppl. 2):S17-S22.

[31] **Jafri, MS, J Rice, and RL Winslow** (1998) *Cadiac Ca^{2+} dynamics: the roles of ryanodine receptor adaptation and sarcoplasmic reticulum load.* Biophys J 74:1149-1168.

[32] **Jorgensen, AO, R Broderick, AP Somlyo, and AV Somlyo** (1988) *Two structurally distinct calcium storage sites in rat cardiac sarcoplasmic reticulum: an electron microprobe analysis study.* Circ Res 63:1060-1069.

[33] **Kawano, S, Y Hirayama, and M Hiraoka** (1995) *Activation mechanism of Ca^{2+}-sensitive transient outward current in rabbit ventricular myocytes.* J Physiol 486(3):593-604.

[34] **Li, D, J Feng, Z Wang, and S Nattel** (1999) *The effects of experimental heart failure on atrial cellular and ionic electrophysiology.* submitted.

[35] **Li, GR, J Feng, Z Wang, B Fermini, and S Nattel** (1995) *Comparative mechanisms of 4-aminopyridine-resistant I_{to} in human and rabbit atrial myocytes.* Am J Physiol 269(Heart Circ Physiol 38):H463-H472.

[36] **Li, GR, and S Nattel** (1997) *Properties of human atrial I_{Ca} at physiological temperatures and relevance to action potential.* Am J Physiol 272(Heart Circ Physiol 41):H227-H235.

[37] **Liu, D-W, and C Antzelevitch** (1995) *Characteristics of the delayed rectifier current (I_{Kr} and I_{Ks}) in canine ventricular epicardial, midmyocardial, and endocardial myocytes: a weaker I_{Ks} contributes to longer action potential of the M cell.* Circ Res 76:351-365.

[38] **Liu, L, and S Nattel** (1997) *Differing sympathetic and vagal effects on atrial fibrillation in dogs: role of refractoriness heterogeneity.* Am J Physiol 273(Heart Circ Physiol 42):H805-H816.

[39] **Lindblad, DS, CR Murphey, JW Clark, and WR Giles** (1996) *A model of the action potential and underlying membrane currents in a rabbit atrial cell.* Am J Physiol 271(Heart Circ Physiol 40):H1666-H1696.

[40] **Luo, CH, and Y Rudy** (1991) *A model of the ventricular cardiac action potential: depolarization, repolarization, and their interaction.* Circ Res 68:1501-1526.

[41] **Luo, CH, and Y Rudy** (1994) *A dynamic model of the cardiac ventricular action potential. II. Afterdepolarizations, triggered activity, and potentiation.* Circ Res 74:1097-1113.

[42] **Marquardt, DW** (1963) *An algorithm for least-squares estimation of nonlinear parameters.* J Soc Ind Appl Math 11:431-441.

[43] **McAllister, RC, D Noble, and RW Tsien** (1975) *Reconstruction of the electrical activity of cardiac Purkinje fibres.* J Physiol (Lond) 251(1):1-59.

[44] **McPherson, PS, and KP Campbell** (1993) *Characterization of the major brain form of the ryanodine receptor/Ca2+ release channel.* J Biol Chem 268:19785-19790.

[45] **Moe, GK** (1962) *On the multiple wavelet hypothesis of atrial fibrillation* Arch Int Pharmacodyn Ther 140:183-188.

[46] **Morillo, CA, GJ Klein, DL Jones, and CM Guiraudon** (1995) *Chronic rapid atrial pacing: structural, functional, and electrophysiological characteristics of a new model of sustained atrial fibrillation.* Circulation 91:1588-1595.

[47] **Muraki, K, Y Imaizumi, M Watanabe, Y Habuchi, and WR Giles** (1995) *Delayed rectifier K^+ current in rabbit atrial myocytes.* Am J Physiol 269(Heart Circ Physiol 38):H524-H532.

[48] **Nattel, S, T Hadjis, and M Talajic** (1994) *The treatment of atrial fibrillation: an evaluation of drug therapy, electrical modalities and therapeutic considerations.* Drugs 48:345-371.

[49] **Nattel, S, G Bourne, and M Talajic** (1997) *Insights into mechanisms of antiarrhythmic drug action from experimental models of atrial fibrillation.* J Cardiovasc Electrophysiol 8(4):469-480.

[50] **Nattel, S, M Courtemanche, and Z Wang** (1997) *Functional and ionic mechanisms of antiarrhythmic drugs in atrial fibrillation.* In: RH Falk, PJ Podrid, eds. Atrial Fibrillation: Mechanisms and Management. Philadelphia: Lippincott-Raven Publishers, 75-90.

[51] **Noble, D, and SJ Noble** (1984) *A model of the sino-atrial node electrical activity based on a modification of the DiFrancesco-Noble (1984) equations.* Proc R Soc Lond B Biol Sci B222:295-304.

[52] **Nygren, A, C Fiset, L Firek, JW Clark, DS Lindblad, RB Clark, and WR Giles** (1998) *Mathematical model of an adult human atrial cell: the role of K^+ currents in repolarization.* Circ Res 82(1):63-81.

[53] **O'Rourke, B, DA Kass, GF Tomaselli, S Kääb, R Tunin, and E Marbán** (1999) *Mechanisms of altered excitation-contraction coupling in canine tachycardia-induced heart failure, I: experimental studies.* Circ Res 84:562-570.

[54] **Rardon, DP, DC Cefali, RD Mitchell, SM Seiler, and LR Jones** (1989) *High molecular weight proteins purified from cardiac junctional sarcoplasmic reticulum vesicles are ryanodine-sensitive calcium channels.* Circ Res 64:779-789.

[55] **Rasmusson, RL, JW Clark, WR Giles, K Robinson, RB Clark, EF Shibata, and DL Campbell** (1990) *A mathematical model of electrophysiological activity in a bullfrog atrial cell.* Am J Physiol 259(Heart Circ Physiol 28):H370-H389.

[56] **Shorofsky, SR, R Aggarwal, M Corretti, JM Baffa, JM Strum, BA Al-Seikhan, YM Kobayashi, LR Jones, WG Wier, and CW Balke** (1999) *Cellular mechanisms of altered contractility in the hypertrophied heart: big hearts, big sparks.* Circ Res 84:424-434.

[57] **Sun, X-H, F Protasi, M Takahashi, H Takeshima, DG Ferguson, and C Franzini-Armstrong** (1995) *Molecular architecture of membranes involved in excitation-contraction coupling of cardiac muscle.* J Cell Biology 129:659-671.

[58] **Sun, H, N Leblanc, and S Nattel** (1997) *Mechanisms of inactivation of L-type calcium channels in human atrial myocytes.* Am J Physiol 272(Heart Circ Physiol 41):H1625-H1635.

[59] **Tieleman, RG, CDJ De Langen, IC Van Gelder, PJ de Kam, J Grandjean, KJ Bel, MCEF Wijfels, MA Allessie, and HJGM Crijns** (1997) *Verapamil reduces tachycardia-induced electrical remodeling of the atria.* Circulation 95:1945-1953.

[60] **Tieleman, RG, IC Van Gelder, HJGM Crijns, PJ de Kam, MP Van Den Berg, J Haaksma, HJ Van Der Woude, and MA Allessie** (1998) *Early recurrences of atrial fibrillation after electrical cardioversion: a result of fibrillation-induced electrical remodeling of the artria?* J Am Coll Cardiol 31:167-73.

[61] **Varghese, A, and GR Sell** (1997) *A conservation principle and its effect on the formulation of Na-Ca exchanger current in cardiac cells.* J Theor Biol 189:33-40.

[62] **Vassort, G, and J Alvarez** (1994) *Cardiac T-type calcium current: pharmacology and roles in cardiac tissues.* J Cardiovasc Electrophysiol 5:376-393.

[63] **Victorri, B, A Vinet, FA Roberge, and JP Drouhard** (1985) *Integration methods for action potential reconstruction using Hodgkin-Huxley-type models.* Comp Biomed Res 18:10-23.

[64] **Wang, Z, LC Pelletier, M Talajic, and S Nattel** (1990) *Effects of flecainide and quinidine on human atrial action potentials:role of rate-dependence and comparison with guinea pig, rabbit, and dog tissues.* Circulation 82:274-283.

[65] **Wang, Z, B Fermini, and S Nattel** (1993) *Sustained depolarization-induced outward current in human atrial myocytes: evidence for a novel delayed rectifier potassium current similar to Kv1.5 cloned channel currents.* Circ Res 73:1061-1076.

[66] **Wang, Z, B Fermini, and S Nattel** (1993) *Delayed rectifier outward currents and repolarization in human atrial myocytes.* Circ Res 73:276-285.

[67] **Wang, Z, B Fermini, and S Nattel** (1994) *Rapid and slow components of delayed rectifier current in human atrial myocytes.* Cardiovasc Res 28:1540-1546.

[68] **Wang, H-S, JE Dixon, and D McKinnon** (1997) *Unexpected and differential effects of Cl^- channel blockers on the Kv4.3 and Kv4.2 K^+ channels.* Circ Res 81:711-718.

[69] **Wijffels, MC, CJ Kirchhof, R Dorland, and MA Allessie** (1995) *Atrial fibrillation begets atrial fibrillation. A study in awake chronically instrumented goats.* Circulation 92(7):1954-1968.

[70] **Wilders, R, HJ Jongsma, and ACG van Ginneken** (1991) *Pacemaker activity of the rabbit sinoatrial node: a comparison of mathematical models.* Biophys J 60:1202-1216.

[71] **Yue, L, J Feng, GR Li, and S Nattel** (1996) *Transient outward and delayed rectifier currents in canine atrium: Properties and role of isolation methods.* Am J Physiol 270(Heart Circ Physiol 39):H2157-H2168.

[72] **Yue, L, J Feng, GR Li, and S Nattel** (1996) *Characterization of an ultrarapid delayed rectifier potassium channel involved in canine atrial repolarization.* J Physiol (Lond) 496:647-662.

[73] **Yue, L, J Feng, R Gaspo, GR Li, and S Nattel** (1997) *Ionic remodeling underlying action potential changes in a canine model of atrial fibrillation.* Circ Res 81:512-525.

[74] **Zygmunt, AC** (1994) *Intracellular calcium activates a chloride current in canine ventricular myocytes.* Am J Physiol 267(Heart Circ Physiol 36):H1984-H1995.

[75] **Zygmunt, AC, DC Robitelle, and GT Eddlestone** (1997) *I_{to1} dictates behavior of $I_{Cl(Ca)}$ during early repolarization of canine ventricle.* Am J Physiol 273(Heart Circ Physiol 42):H1096-H1106.

Acknowledgements

This research and the preparation of this manuscript were realized thanks to the efforts and assistance of others. My sincerest appreciation goes to my principal thesis supervisor, Dr. Marc Courtemanche, for his indomitable patience and generosity. His wisdom and knowledge remain an inspiration and motivation.

My deep appreciation also goes to my cosupervisor, Dr. Stanley Nattel, Director of the Research Center at the Montreal Heart Institute, whose laboratory and unique approach to cardiac electrophysiology has provided the perfect environment for my research. His guidance and suggestions have been invaluable.

I would also like to thank Normand Leblanc and Alain Vinet, who have accepted to be members of my thesis committee and critically reviewed this manuscript. Their constructive suggestions have improved this work and were greatly appreciated.

I also thank Lixia Yue, Jianlin Feng, and Danshi Li for providing the experimental data used in this study.

Finally, I thank my family for always being there.